recycling

MDPI

Article

Valorization Diagnosis of Roasted Pyrite Ashes Wastes from the Iberian Pyrite Belt

Juan Antonio Ramírez-Pérez [1], Manuel Jesús Gázquez-González [2] and Juan Pedro Bolívar [1,*]

[1] Department of Integrated Sciences, Center for Natural Resources, Health and Environment (RENSMA), University of Huelva, 21071 Huelva, Spain; juan.ramirez@dci.uhu.es
[2] Department of Applied Physics, Instituto de Investigación Marina (INMAR), University of Cádiz, 11510 Puerto Real, Spain; manueljesus.gazquez@uca.es
* Correspondence: bolivar@uhu.es

Abstract: The Iberian Pyrite Belt (IPB) contains the world's largest massive sulfide deposit, and, due to extensive mining developed during the last 200 years, large amounts of mining waste have been abandoned in this area, with roasted pyrite ash being the focus of this study. Polymetallic mining is also classified as a NORM (naturally occurring radioactive material) activity, thus the main objective of this work was to develop a radiological and physicochemical characterization of this waste (mineral phases, elemental and radionuclide concentrations) in order to perform a valorization diagnosis of this material. The composition of this waste strongly depends on its origin (mine), and is mainly formed by iron oxides (hematite, Fe_2O_3) and heavy metals and metalloids such as As, Pb, Zn, and Cu, in levels 2–4 orders of magnitude higher than those of undisturbed soils, depending on each particular element. However, the average natural radionuclide levels are similar to those of unperturbed soils (around 30 Bqkg^{-1} of ^{238}U-series, 50 Bqkg^{-1} of ^{232}Th, and 70 Bqkg^{-1} for ^{40}K), thus they are below the limits established by European Union regulations to require radiological control during their future valorization. As the main potential applications of roasted pyrite ash, the valorization diagnosis indicates that it can be used as a source of Fe ($FeCl_3$ or $FeSO_4$), or an additive in the manufacturing of cements, pigments, etc.

Keywords: mining wastes; Iberian Pyrite Belt; roasted pyrite ashes; valorization diagnosis; radionuclides

Academic Editor: Jack Groppo

Received: 26 February 2025
Revised: 14 April 2025
Accepted: 31 May 2025
Published: 4 June 2025

Citation: Ramírez-Pérez, J.A.; Gázquez-González, M.J.; Bolívar, J.P. Valorization Diagnosis of Roasted Pyrite Ashes Wastes from the Iberian Pyrite Belt. *Recycling* **2025**, *10*, 112. https://doi.org/10.3390/recycling10030112

1. Introduction

The Iberian Pyrite Belt (IPB) is in the southwestern region of the Iberian Peninsula, spanning parts of Portugal and Spain. This area is recognized for hosting the world's largest concentration of massive sulfide deposits [1]. The original reserves have been estimated to hold about 1700 Mt [2]. Mining and metallurgical activities in this region date back to around 4500 BC and continue to the present day [3]. Intense mineral extraction and processing, especially during the late 19th and early 20th centuries, led to the accumulation of vast amounts of mining waste across various sites along the Odiel and Tinto River basins. These areas are often referred to as "legacy sites". In addition, many galleries and pit/pit lakes were also abandoned, which are weathered, and, as a consequence, acid mine drainage (AMD) is produced due to the very low neutralization capacity of the rocks from this geographical area [4].

Many of these mining residues contain elevated concentrations of toxic metals and metalloids, including arsenic and heavy metals. Additionally, these metallic mining activities have been qualified as naturally occurring radioactive material (NORM) wastes, as defined

by European Directive 2013/35/UE and Spanish regulations. Under European Union guidelines, NORM wastes can pose radiological risks to the public and workers, requiring their radioactive characterization, classification, and management through a robust quality control framework [5,6]. These legacy sites can present significant environmental, safety, and public health challenges, particularly due to the fact that they are frequently located near populated areas and ecologically sensitive aquatic systems, as in the studied case [7,8]. Little research has been conducted on the presence of naturally occurring radionuclides in mining residues, except for uranium mining [9]. This underscores the need for radiological assessments and the dissemination of information regarding these materials.

Aqueous acid leachates are released from these waste deposits, since they are strongly affected by the oxidation of the sulfide contained in them, thereby acidifying the aqueous medium and releasing different chemical species, many of which are highly toxic heavy metals and metalloids (As) that are generally untreated, generating significant environmental problems [4]. Clear examples of this are the Odiel and Tinto rivers, whose basins have a high percentage belonging to the IPB, discharging in the common estuary of Huelva, with the Odiel saltmarshes being a UNESCO biosphere reserve. Due to the fact that these rivers receive extremely high levels of pollutants from multiple water streams affected by AMD (a pH of about 2 and 3 for the Tinto and Odiel rivers, respectively), their waters contain elevated concentrations of dissolved metals, sulfates, and radioactive elements such as uranium (U) and thorium (Th). The Tinto and Odiel rivers flow into their common estuary, called "Ría de Huelva" or Huelva Estuary, which is one of the most polluted in the world due to the vast annual flow of dissolved elements that are transported from these rivers into this estuary [10].

There is currently great interest in carrying out an evaluation and inventory of the different types of abandoned mining wastes existing in this geographical area, with the aim of remediating them or, if possible, valorizing them in different commercial applications, which was analyzed in this study. One of the main mining wastes is roasted pyrite (Fe_2S), which comes from a process that converts the sulfur in SO_2 to produce sulfuric acid, generating a solid calcined product ("ashes"), consisting mainly of iron oxides and other non-volatile oxidized elements contained in the original ore (Cu, Pb, Zn, etc.).

During the industrial process, firstly, the roasting process converts the pyrite concentrate into solid oxides and sulfur dioxide by heating up the ore to 600–1000 °C [11]:

$$2FeS_2 + 5.5O_2 \rightarrow Fe_2O_3 + 4SO_2. \quad (1)$$

It is then cooled to 320–400 °C, separating the gaseous fraction from the coarse particles using cyclones. Then, the finest suspended particles remaining in the hot gas are removed by electrostatic precipitation. The gas is cooled down to 65 °C, where dissolved SO_2 is removed by an extraction column. Subsequently, the gas is cooled down again to 40 °C and, by using wet electrostatic precipitators, the fine particles and acid aerosols are removed. Finally, the sulfur dioxide is oxidized to SO_3, which is combined with water, producing sulfuric acid [11]. In this process, a solid waste called "roasted pyrite" is generated (Figure 1B). This sulfuric acid is used to lixiviate Cu from copper ores, mainly containing chalcopyrite ($CuFeS_2$) and chalcocite (Cu_2S). The obtained leachate is conducted into "cementation" areas using numerous channels filled with iron scrap, enabling the precipitation of Cu by the ionic replacement of Fe. Cement Cu has been reported to reach grades of 60–90% Cu [2].

Figure 1. (**A**) Iberian Pyrite Belt and location of the studied mines; (**B**) an example of analyzed roasted pyrite ashes from Sotiel Coronada.

Considering the potential environmental and human health problems related to this mining waste eliminated in uncontrolled repositories, the main objective of this work was to perform a thorough radioactive and multi-elemental characterization of roasted pyrite ash wastes located at different representative mines from the IPB, along with an evaluation of their radiological risks. Additionally, different valorization lines were proposed to recycle these wastes.

2. Materials and Methods

2.1. Study Area, Samplings, and Sample Pre-Treatment

Considering the roasted pyrite ashes produced historically, the following largest mining zones were selected and sampled: Sotiel Coronada (SC), Cueva de la Mora (CM), Herrerías (HE), Lagunazo (LA), Zarza-Perrunal (ZP), San Telmo (ST), and Riotinto (RT) (see Figure 1A). An example of the waste from Sotiel Coronada mine is shown in Figure 1B. Sampling was carried out in situ during November-December 2023, previously removing the first 5 cm to ensure that the samples were not affected by weathering. Approximately 1 kg per sample was extracted at each sampling point with a shovel and stored for subsequent pre-treatment (drying, grinding, etc.). The samples studied and their locations are listed in Table 1.

Table 1. Samples studied and their locations. ETRS89/UTM 29N coordinates. Sotiel Coronada (SC; 5 samples), Cueva de la Mora (CM; 3 samples), Herrerías (HE), Lagunazo (LA), Zarza-Perrunal (ZP), San Telmo (ST), and Riotinto (RT; 2 samples).

Sample	Abscissa (m E)	North (m N)
SC1	689,628	4,168,479
SC2	689,640	4,168,346
SC3	689,401	4,168,293
SC4	689,181	4,168,324
SC5	688,987	4,168,194
CM1	692,431	4,183,624
CM2	692,398	4,183,648
CM3	692,326	4,183,857
HE1	649,878	4,164,799

Table 1. *Cont.*

Sample	Abscissa (m E)	North (m N)
LA1	661,691	4,165,465
ZP1	689,141	4,174,853
ST1	679,214	4,185,844
RT1	714,920	4,175,002
RT2	715,030	4,1753,66

2.2. Physicochemical Parameters

To study the physicochemical properties of the samples, the pH and electrical conductivity (EC) were measured in the laboratory. To this end, about 10 g of a sample was deposited in a conical Falcon tube together with 25 mL of distilled water (L/S ratio = 2.5) and agitated in a rotary mixer for 10 min. Finally, the solid and liquid fractions were separated by centrifugation, and the physicochemical parameters of the liquid layer were measured with a CRISON model MM40+ multiparametric sensor.

2.3. Multi-Elemental Composition

The elemental composition of the samples was determined by the certified Activation Laboratories Ltd. (ACTLABS) in Ontario, Canada. Measurements were performed using inductively coupled plasma mass spectrometry (ICP-MS) and inductively coupled plasma optical emission spectrometry (ICP-OES). To ensure near-total dissolution, a mixture of four concentrated acids (hydrochloric, nitric, perchloric, and hydrofluoric) was employed. For the ICP-OES analysis, a Varian 735ES instrument was used, while an ELAN 9000 spectrometer was used for ICP-MS measurements. Quality control procedures included the use of replicates, blanks, and certified reference materials (CRM): OREAS 903, 96, 520, 683, 70b, 620, and 603c.

To determine the concentrations of major elements, X-ray fluorescence (XRF) analyses were conducted, using a PANalytical ZETIUM sequential model at the Research, Technology, and Innovation Center (CITIUS) of the University of Seville, Spain. The equipment features a 4 kW X-ray tube with a rhodium anode and a front window, two detectors (flux and scintillation), and five analytical crystals (PX1, PE 002, LIF 200, Ge 111, and LIF 220). For each dry sample, a 1.5 g aliquot was prepared.

2.4. Mineralogy

The mineralogical analysis was conducted by X-Ray diffraction. The pre-treatment consisted of mixing the sample with an internal standard of 12% Zincite (ZnO), in order to determine the amorphous fraction of the material by applying Rietveld's methodology. Once the samples were homogenized with this internal standard, they were sent to CITIUS for analysis. A Bruker powder diffractometer model D8 ADVANCE A25 was used, with Bragg–Brentano geometry, a Cu tube, Soller slits, a motorized primary slit, a linear detector, and optional sample rotation. In addition, it included a 90-position programmable sample changer. A semi-quantitative method was applied, with the following conditions: $\Delta 2\theta$ = 3–70°; step = 0.015°; t = 0.1 s; tube conditions: 40 kV and 30 mA; divergence slit: fixed 0.5°; sample rotated at 30 rpm; nickel filter. Once the results were received from CITIUS, the diffraction spectra were analyzed qualitatively and quantitatively using DIFFRAC.EVA and DIFFRAC.TOPAS, applying Rietveld's method in the latter case [12]. PROFEX software was also used for determining a preliminary study of the crystalline phases of the samples.

2.5. Radioactive Characterization

The radioactive characterization was conducted using two low-level radiometric techniques: alpha-particle spectrometry with PIPS-type silicon detectors and gamma spectrometry with germanium detectors. For alpha-particle spectrometry, a sequential extraction method was used to isolate actinides (primarily thorium and uranium isotopes) and ^{210}Po. This method, known as the tributyl phosphate (TBP) method, involved the following steps: firstly, tracers ^{229}Th, ^{232}U, and ^{209}Po were added to assess process yield. Approximately 0.5 g of the sample was dissolved in closed vessels. Subsequently, TBP isolation was carried out to separate polonium, uranium, and thorium. Finally, electrodepositions of uranium and thorium and self-deposition of polonium were performed [13]. The alpha emitters analyzed included ^{238}U, ^{235}U, ^{234}U, ^{232}Th, ^{230}Th, and ^{210}Po.

Gamma spectrometry was used to determine the activity concentrations of gamma-emitting radionuclides in the samples. A high-purity germanium (HPGe) detector with extended range (XtRa) and a thin beryllium window was employed to detect low-energy emissions down to approximately 20 keV. To minimize natural background radiation, a nitrogen-purged shielding system replaced the air within the shielding, effectively removing radon. The detector demonstrated an efficiency of 38.4% at 1332 keV compared with a $3'' \times 3''$ NaI(Tl) detector. It also had a full width at half maximum (FWHM) of 1.74 keV at 1332 keV and 0.88 keV at 122 keV, with a Compton-to-peak ratio of 67.5:1 [14,15]. Gamma emitters analyzed included ^{234}Th (63.29 keV), ^{226}Ra (186.2 keV), ^{210}Pb (46.52 keV), and ^{40}K (1460.83 keV). Radionuclides ^{228}Ra and ^{228}Th were also examined due to their secular equilibrium with gamma emitters ^{228}Ac (911 keV) and ^{212}Pb (238 keV), respectively.

For every ten samples, quality control for both techniques included the use of blanks, replicates, and certified reference materials (IAEA-375 and IAEA-327), along with participation in intercomparison exercises.

2.6. Emanation Factor and Exhalation Rate

The emanation factor and the exhalation ratio were measured by placing the residue in an accumulation chamber (polypropylene box). Once sealed, the radon concentration inside was measured and the accumulation curve was recorded (Figure 2), extracting the air from inside and returning it after the measurement, being recycled through the Rn monitor (RAD7 or ARAD RTM) [16]. The accumulation curve follows the expression [17]:

$$C(t) = C_{sat}(1 - e^{-t\lambda ef}), \quad (2)$$

where C_{sat} is the saturation concentration and λ_{ef} is the effective time constant, defined as the sum of the radon decay constant (λ_{Rn}), the leakage loss constant (λ_f), and the back-diffusion constant (λ_b). By performing a fitting of the experimental data to the curve of Equation (2), we can calculate both parameters. In this way, the emanation factor (ε) and the exhalation rate (E_0) can be obtained from the following expressions [17]:

$$\varepsilon = (\lambda_{ef}\, C_{sat} V)/(\lambda_{Rn} C_{Ra} m); \quad (3)$$

$$E_0 = (\lambda_{ef}\, C_{sat} V)/S, \quad (4)$$

where V is the accumulation volume (including the volume of the Rn detector), S is the exhalation surface of the sample, and C_{Ra} is the ^{226}Ra activity concentration of the material under testing.

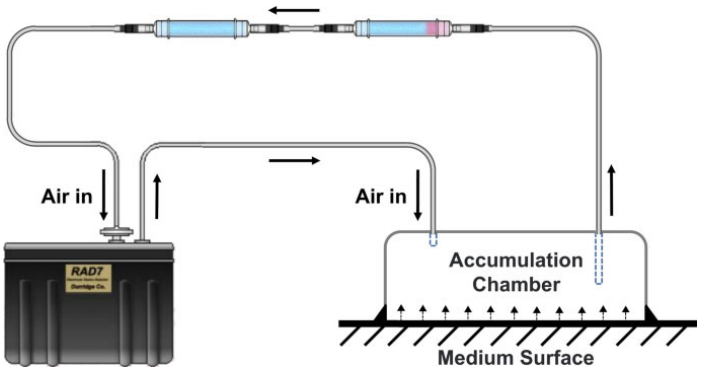

Figure 2. Diagram of the accumulation chamber and the sample placed inside it, recycling the air through the radon monitor.

2.7. Radiological and Pollution Indexes

A key index used to assess radioactive hazards is radium equivalent activity (Ra_{eq}). This parameter consolidates the activity concentrations of ^{238}U, ^{232}Th, and ^{40}K into a single value, accounting for the external radiation hazards posed by these radionuclides and their progeny in secular equilibrium. Ra_{eq} is designed to represent the equivalent activity concentration that would result in the same external dose, as defined by the following expression [18,19]:

$$Ra_{eq}\ (Bqkg^{-1}) = C_U + 1.43C_{Th} + 0.077C_{K,} \quad (5)$$

where C_U, C_{Th}, and C_K represent the activity concentrations of ^{238}U, ^{232}Th, and ^{40}K, respectively, expressed in $Bqkg^{-1}$. The United States Environmental Protection Agency (USEPA) has established a threshold value of 370 $Bqkg^{-1}$ for materials to be considered safe for use in any application [20].

The external hazard index (H_{ex}) estimates the radiation dose from external gamma exposure due to natural radionuclides present in building materials, particularly in enclosed spaces such as wells. It is calculated as follows [21,22]:

$$H_{ex} = C_U/370 + C_{Th}/259 + C_K/4810. \quad (6)$$

The effective dose will be lower than 1 mSv/y if Hex is lower than 1 [20]. Additionally, the European Union directive "Radiation Protection 112" introduces the activity concentration index (Ic) to assess gamma radiation emitted by building materials. This index is determined using the following equation [5]:

$$Ic = C_{Ra}/300 + C_{Th}/200 + C_K/3000, \quad (7)$$

where C_{Ra} represents the activity concentration of 226Ra, expressed in $Bqkg^{-1}$. The Ic value should remain below 1 for construction materials that include naturally radioactive substances such as fly ash, phosphogypsum, and slag. For surface materials or those with limited applications, such as tiles and boards, the acceptable Ic threshold can be up to 6.

Finally, to compare the activity concentrations of radionuclides with those of unperturbed reference soil from the same geographical region ("background"), the concentration factor (CF_i) for a specific radionuclide "i" is calculated using the following equation:

$$CF_i = C_i/Cr_i, \quad (8)$$

where C_i is the activity concentration of radionuclide "i" (in $Bqkg^{-1}$), and Cr_i is the reference activity concentration for the same radionuclide in the background soil in $Bqkg^{-1}$.

In this study, ^{238}U and ^{232}Th are used as reference radionuclides, with background activity concentrations of 33.29 $Bqkg^{-1}$ and 42.52 $Bqkg^{-1}$, respectively [23].

It is also necessary to quantify the grade of pollution due to metal and metalloid elements (As, Cd, Cr, Cu, Ni, Pb, and Zn), comparing their concentrations with those obtained for unpolluted soils (background). This toxicity is compared to the composition of an uncontaminated background. The contamination factor (C^i) of an element "i" is established by the following equation [24]:

$$C^i = (C^i)_{sample}/(C^i)_{background}, \quad (9)$$

where $(C^i)_{sample}$ is the "i" element concentration in the sample and $(C^i)_{background}$ is the background concentration of the same element. The degree of contamination (C_d) is the sum of all contamination factors of the different heavy metal (or radionuclides) and helps for a better assessment of the full pollution of the materials. Depending on C^i and C_d, risk indexes are established in Table 2 [25]:

Table 2. Levels of pollution according to the ranges of contamination factor C^i and contamination degree C_d.

Contamination Factor	Degree of Contamination	Contamination Level
$C^i < 1$	$C_d < 8$	Low
$1 \leq C^i < 3$	$8 \leq C_d < 16$	Moderate
$3 \leq C^i < 6$	$16 \leq C_d < 32$	Considerable
$C^i \geq 6$	$C_d \geq 32$	Very high

The potential ecological risk factor for a given toxic element (E^i) (see Table 3) can also be defined, which allows evaluating the potential toxicity associated with its presence in the soil. It is expressed as follows:

$$E^i = C^i \cdot T^i, \quad (10)$$

where T^i is the toxic response factor for a given element. In the same way, the ecological risk index (RI) is defined as the sum of all E^i of the elements under study. Its evaluation criteria are shown in Table 3 [25].

Table 3. Contamination levels according to E^i for I element and RI values for sample.

Potential Risk	Ecological Risk Index	Risk Level
$E^i < 40$	RI < 150	Low
$40 \leq E^i < 80$	$150 \leq$ RI < 300	Moderate
$80 \leq E^i < 160$	$300 \leq$ RI < 600	High
$160 \leq E^i$	RI $\geq$ 600	Very high/extreme

The background concentrations established for the analyzed elements [26] and their toxic response factors are in Table 4 [25] as follows:

Table 4. Reference values established for the different elements: background concentrations in ppm and toxic response factors (dimensionless) T^i [25,26].

Index	As	Cd	Cr	Cu	Ni	Pb	Zn
$(C^i)_{background}$ (ppm)	4.8	0.09	92	28	47	17	67
T^i	10	30	2	5	5	5	1

2.8. Pollutant Mobility

To determine the mobility of elements that pose a potential risk to the environment, a leaching analysis was performed in accordance with the UNE-EN 12457-4 standard, titled "Characterization of waste-Leaching-Compliance test for leaching of granular waste materials and sludges—Part 4: One stage batch test at a liquid to solid ratio of 10 L/kg for materials with particle size below 10 mm" [27]. This guideline considers leaching as the release of soluble constituents, highlighting contact with water as the main release mechanism, which could represent an environmental risk during the waste reuse or disposal phases. The aim of this procedure is to identify the properties of waste leachates, providing data on the aqueous leaching of granular waste and sludge. This European standard is applied to materials with particles smaller than 10 mm and is designed for the investigation of inorganic components present in the waste. After 24 h agitation and filtration on a 0.45 μm membrane, the resulting leachates were measured by ICP-MS and ICP-OES. Furthermore, using ion chromatography, the concentrations of the different anions found in the water after forced leaching with water can be measured.

In addition, the transfer factor (TF) into the leaching liquid was calculated for each element. TF is defined as the mass released from element "x" in the water leachate in relation to its mass contained in the solid. It is calculated according to the expression:

$$TF\ (\%) = 100 \cdot C_{lix} / C_{sow}, \quad (11)$$

where C_{lix} is the leachate concentration in the water and C_{sow} is the solid concentration of element "x" in the original waste. Both concentrations are in μg/g of the original waste. Furthermore, the affinity of an element to the solid phase relative to the liquid phase is defined by the partition coefficient K_d [28]:

$$K_d\ (L/kg) = C_s / (C_l), \quad (12)$$

where C_s is the solid concentration of the element after equilibrium, and C_l is the concentration of the leached element after equilibrium. It can be seen that:

$$K_d\ (L/kg) = V_{lix} / (M_s \cdot TF), \quad (13)$$

where V_{lix} is the leachate volume, and M_s is the solid mass used for the test.

3. Results and Discussion

3.1. Physicochemical Parameters

Table 5 shows the pH and EC values obtained for the samples. In general, roasted pyrite ashes showed high acidity, with a pH interval from 2.5 to 4.0. The lowest and the highest values belonged to SC3 and SC5, with 2.52 and 4.01 values, respectively. On the other hand, EC values were more varied among the mines of origin. The mine with the highest electrical conductivity value was Sotiel Coronada, especially sample SC5, standing out with a value of 5030 μS/cm. The mine with the lowest value was Lagunazo (LA1), with 320 μS/cm. These values raise the possibility of the existence of AMD in the wastes, as the presence of sulfides such as pyrite release sulfuric acid after oxidation and cause the leaching of the heavy metals contained in them. The mean values for pH and EC were 3.27 ± 0.03 and 2080 ± 100 μS/cm, respectively, whereas, for surface unpolluted waters, these values were around 6–8 and 50–500 μS/cm.

Table 5. Physicochemical parameters, pH and CE, of the samples. Sample codes: Sotiel Coronada (SC), Cueva de la Mora (CM), Herrerías (HE), Lagunazo (LA), Zarza-Perrunal (ZP), San Telmo (ST), and Riotinto (RT).

Sample	pH	EC (µS/cm)
SC1	3.04	2420
SC2	3.59	2890
SC3	2.52	3580
SC4	3.21	3080
SC5	4.01	5030
CM1	2.74	2160
CM2	2.61	3160
CM3	3.36	443
HE1	3.29	541
LA1	3.90	320
ZP1	3.80	2440
ST1	2.98	2070
RT1	3.21	636
RT2	3.53	341
Mean	3.27 ± 0.12	2080 ± 390

3.2. Major Elements

Prior to proceeding with the correct valorization diagnosis, it is necessary to determine the major elements (concentrations > 0.1% in general) that characterize the waste (Table 6). Roasted pyrite ashes are mainly composed of iron (Fe = 46.4 ± 0.6% average). These iron values are similar for each type of mine (28–58%), and are generally one order of magnitude higher than those of soils (around 4.0%) [29]. This waste, as expected, presented a low content of S in relation to pyrite (1.23 ± 0.03% on average with low variability when in pyrite around 50%), although exceeding typical S soil values (0.02%) by 2 orders of magnitude [30].

For the rest of the elements, there were more discrepancies depending on the mines of origin. The average concentrations of Al (0.59%), K (0.18%) and Na (0.09%) were lower than the expected soil concentrations in the IPB (8.72% for Al, 1.95% for K, and 0.87% for Na), especially those of the Zarza-Perrunal residue for Al and K. On the other hand, Mg (0.14% on average) and Ti (0.17% on average) concentrations corresponded to the soil (0.26% and 0.24%, respectively) for the Sotiel Coronada wastes, but were lower for the rest [29].

Moreover, for heavy metals/metalloids such as Cu, Pb, Zn, and As, the values obtained for most of the wastes exceeded the values for unperturbed soil by 1-to-3 orders of magnitude ($5.9 \cdot 10^{-3}$% Cu; $6.3 \cdot 10^{-3}$% Pb; $8.3 \cdot 10^{-3}$% Zn; $4.2 \cdot 10^{-3}$% As [29]). Zarza-Perrunal and San Telmo wastes presented the lowest concentrations of these elements, while Sotiel Coronada waste showed the highest concentrations. It is necessary to emphasize the extremely high concentration of Pb obtained in the Lagunazo sample (LA1) (2.1%). Consequently, these wastes have high toxicological implications for the environment [31], but they could be valorized by extracting the Pb content. Similarly, high sulfur levels imply acidity in the area and a possible impact from AMD.

All these major element concentrations are consistent with those of previous studies on roasted ashes located in the Iberian Pyrite Belt. Yesares and collaborators (2023) obtained the following concentrations: Fe 37–50%, S < 5%, Al < 4%, and K < 2%. Moreover, the concentrations of the toxic metals Pb and As are in the range of 0.5–2% [2]. Another study carried out by Oliveira in 2012 on these wastes in Santa Catarina, Brazil, reports that, although there is consistency in elements such as Fe (around 51%) and S (around 1%), there are no such high concentrations for toxic elements, proving to be a problem in IPB [32].

Table 6. Major element concentrations in % for all roasted pyrite ash samples, including the mean and the standard uncertainty of the mean. (*) O was calculated to be close to 100%. Background from soils [26,29,30] and concentration factors for each element (CF) are included.

Sample	Mg	Al	K	Ca	Fe	Zn	S	Pb	Cu	Ti	As	Na	Si	O (*)
SC1	0.15	0.66	0.12	0.48	54.5	1.80	0.70	1.72	0.37	0.47	0.58	0.03	3.02	31.2
SC2	0.25	0.91	0.19	2.08	43.0	2.00	1.73	1.23	0.29	0.32	1.45	0.10	5.21	31.7
SC3	0.40	0.48	0.07	0.61	49.9	1.06	2.20	0.57	0.20	0.34	0.73	0.04	1.68	28.6
SC4	0.40	0.83	0.16	1.75	48.6	1.84	1.25	1.73	0.32	0.24	0.48	0.08	3.02	31.2
SC5	0.55	1.18	0.20	1.60	47.3	1.31	1.73	1.34	0.48	0.35	1.59	0.09	2.53	30.5
CM1	0.04	0.65	0.28	0.03	47.3	0.08	1.41	0.86	0.09	0.09	0.44	0.19	8.15	33.0
CM2	0.03	0.26	0.05	0.27	58.0	0.05	1.26	0.40	0.07	0.01	0.54	0.10	2.36	30.2
CM3	0.02	0.36	0.19	0.03	52.7	0.06	1.03	0.79	0.07	0.08	0.44	0.20	6.08	33.5
HE1	0.04	0.49	0.22	0.01	47.9	0.16	0.99	0.28	0.19	0.07	0.06	0.14	6.76	32.6
LA1	0.01	0.56	0.21	0.01	31.7	0.07	1.08	2.10	0.08	0.13	0.49	0.03	5.26	12.5
ZP1	0.01	0.06	0.03	0.38	50.1	0.01	0.59	0.18	0.04	0.01	0.02	0.03	0.87	30.1
ST1	0.08	1.06	0.39	0.03	44.0	0.02	0.93	0.11	0.05	0.12	0.34	0.04	8.01	31.7
RT1	0.03	0.57	0.3	0.01	27.6	0.07	1.20	1.89	0.2	0.13	1.00	0.03	20.1	38.3
RT2	0.02	0.26	0.17	0.01	46.3	0.12	1.12	1.35	0.17	0.04	0.11	0.13	5.02	31.5
Mean	0.14 ± 0.05	0.59 ± 0.08	0.18 ± 0.03	0.52 ± 0.20	46.4 ± 2.1	0.62 ± 0.21	1.23 ± 0.11	1.39 ± 0.18	0.19 ± 0.04	0.17 ± 0.04	0.59 ± 0.13	0.09 ± 0.02	5.6 ± 1.3	30.5 ± 1.5
Background	0.26	8.72	1.95	0.64	4.01	$8.3 \cdot 10^{-3}$	0.02	$6.3 \cdot 10^{-3}$	$5.9 \cdot 10^{-3}$	0.24	$4.2 \cdot 10^{-3}$	0.87	25.1	42.5
CF	0.07	0.09	0.81	11.5	31.0	74.6	59.7	220.6	32.2	59.0	140.7	0.22	0.72	1.39

3.3. Trace Elements

The concentrations of trace elements (<0.1% = 1000 µg/g) are presented in Figure 3, which were measured by ICP-MS/OES. For the natural radioelements (U and Th), the obtained results resemble those expected for typical soils (2.7 µg/g for U and 10.5 µg/g for Th, respectively), with even lower values in some cases [26]. It is worth mentioning the San Telmo waste, ST1, where the uranium concentration stood out for its high value (12.1 µg/g) compared with the other wastes, which was one order of magnitude higher.

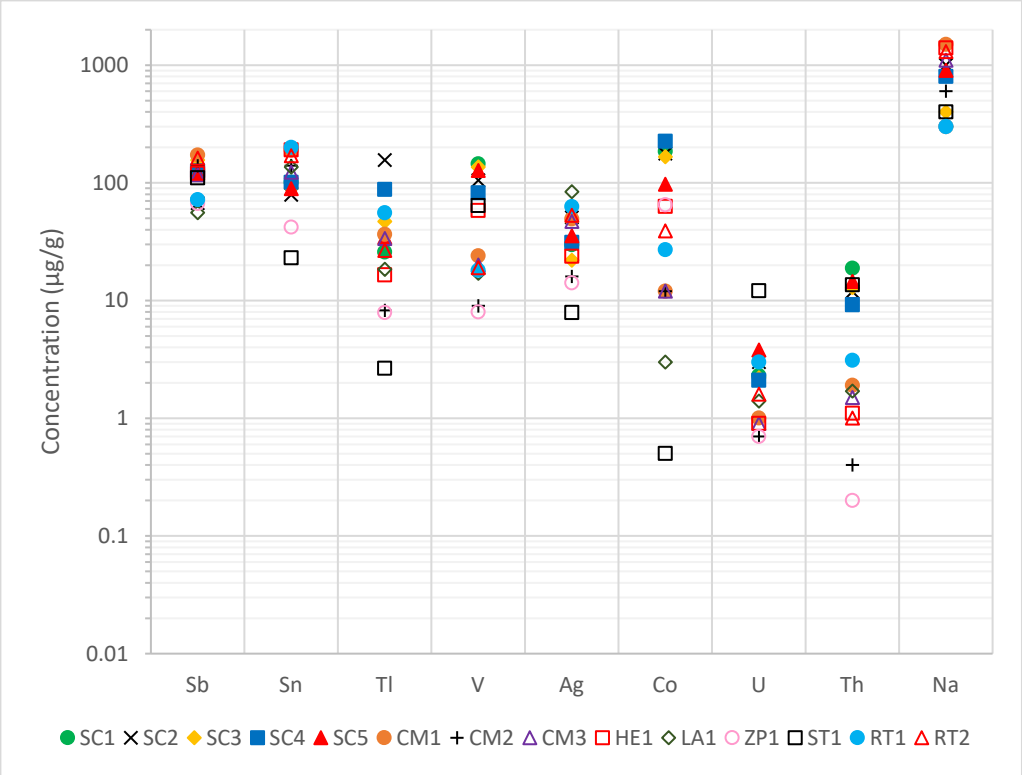

Figure 3. Trace elements concentrations in µg/g for all roasted pyrite ash samples.

The obtained Sb values exceeded the expected value for soils in the IPB of 6.32 µg/g by one order of magnitude. The obtained concentrations were in the range between 55.8 µg/g and 172 µg/g. There is a potential contamination problem due to this element, which would need to be studied for feasibility of extraction and recovery [33]. Furthermore, thallium concentrations exceeded, on average (40 µg/g), by two orders of magnitude the typical value in this area (0.7 µg/g) [29]. Tl is a heavy metal with extreme biotoxicity, being even more dangerous for living organisms than As, Cd, or Pb, producing high contamination in the environment [34].

On the other hand, V and Co concentrations were similar to those expected for soils (68 µg/g and 19 µg/g, respectively), although concentrations were slightly higher in the latter. It is necessary to note the case of the Sotiel Coronada wastes, where vanadium concentrations were higher than the rest and cobalt concentrations were one order of magnitude higher than expected for the other mines. It should also be noted that, in general, all wastes exceeded the soil Sn concentration of 1.87 µg/g by two orders of magnitude, with a mean value of 120 µg/g [29].

The average silver concentration of 37.6 µg/g, being two orders of magnitude above typical soil, raises significant implications from an economic point of view. Depending on the volume of waste and processing costs, there is an opportunity for extraction and

valorization. Moreover, this result considers the historical past of most of the mines, where the main extraction was silver in that area in ancient times [35].

It is necessary to point out that differences in concentrations between mines may be due to the presence of host minerals in the deposit, such as ilmenites (for V) or monazites (for Th), also due to different roasting conditions between mines or interactions with the environment. As the raw materials have different properties at each mine, the roasted pyrites will also have different concentrations. In addition, the mining process has undergone changes over time (one century), thus the methods have been refined, and it is possible that, in the processing, certain differences may be detected in each waste. Lastly, the results are similar to those obtained in the Yesares and Oliveira studies mentioned above [2,32].

3.4. Rare Earth Elements

Another main feature to be studied are rare earth elements (REEs). These elements usually have concentrations of several orders of magnitude in relation to each other depending on the mineral. Therefore, a standardization to chondrite abundance was established in order to better study and understand these elements. Chondrite is a very old mineral that resembles the Earth's crust at the beginning of its formation. The Earth's crust is highly weathered and the elements concentrations are very dependent on each geographical area, thus chondrite is the reference sample of choice in many REE studies. The REE chondrite normalization values are shown in Table 7 [36]:

Table 7. REE chondrite normalization values: Light (La, Ce, Pr, Nd, and Sm), medium (Eu, Gd, Tb, and Dy), and heavy (Ho, Er, Tm, Yb, and Lu). Continental crust concentrations for REEs are also included [37].

Sample	La	Ce	Pr	Nd	Sm	Eu	Gd	Tb	Dy	Ho	Er	Tm	Yb	Lu
Chondrite concentrations (μg/g) [36]	0.237	0.612	0.095	0.467	0.153	0.058	0.205	0.037	0.254	0.057	0.166	0.026	0.170	0.246
Continental crust concentrations (μg/g) [37]	27.1	56.2	-	24.5	4.35	1.09	-	0.62	-	-	-	-	1.83	0.28

Normalized values are shown in Figure 4. There was a high variability of results depending on the type of REE and the mine of origin. Light REEs (LREEs; La, Ce, Pr, Nd, and Sm) had concentrations 1–2 orders of magnitude higher than chondrite, with the highest average values being found at the Sotiel Coronada and San Telmo mines, while the lowest values were found at Zarza-Perrunal. Medium rare earth elements only outnumbered it by 1 in the case of Sotiel Coronada and San Telmo. For the rest, the levels were very similar to those of chondrite, even with lower concentrations in samples from Herrerías (HE1), Lagunazo (LA1), and Zarza-Perrunal (ZP1). Heavy rare earth elements (HREEs; Ho, Er, Tm, Yb, and Lu) concentrations were similar to those of chondrite (range of 2–6), although the values of the San Telmo residue (ST1) stood out, with a value of 26.1 and 32 for Er and Yb, respectively.

High normalized concentrations of REEs were identified, especially for light REEs, which could be due to several reasons, such as REEs often being associated with the presence of iron oxides, such as hematite (Fe_2O_3) [38]. These residues are mainly made up of these iron oxides, hence their reddish color, thus justifying the concentrations obtained. Other studies have shown that REEs are associated with high ^{232}Th contents [39], which was observed in roasted pyrites in San Telmo and Sotiel Coronada.

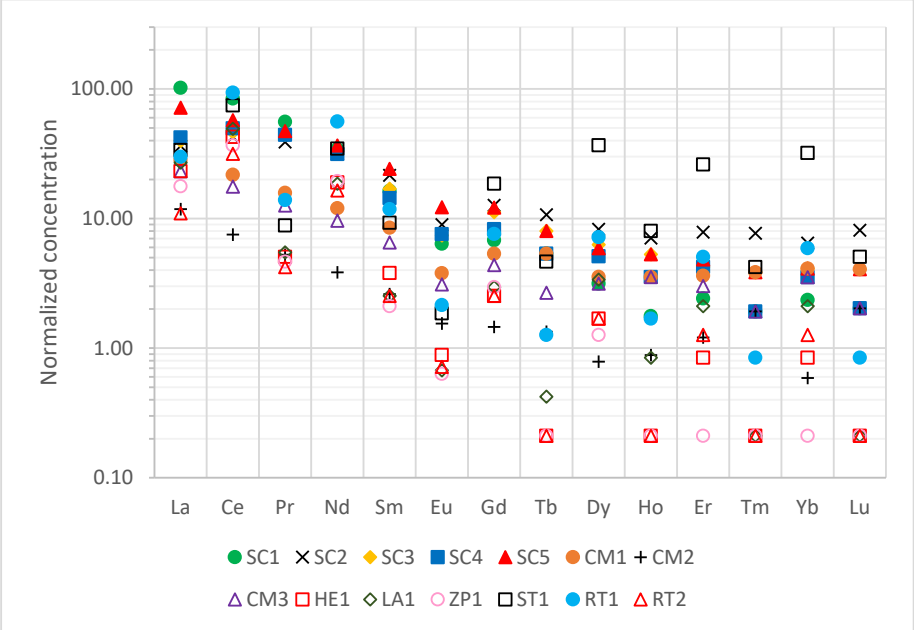

Figure 4. REE concentrations normalized to chondrite.

3.5. Heavy Metals/Metalloids

The concentrations of the highly toxic metals/metalloids are shown in Figure 5a. Figure 5b represents a standardized visual map of the concentrations of these major toxic elements. As can be seen, Cu, Pb, Zn, and As concentrations obtained for most wastes surpassed the expected values for soils in the IPB by 1-to-3 orders of magnitude (300 µg/g Cu; 400 µg/g Pb; 800 µg/g Zn; 200 µg/g As [26]). Sotiel Coronada (SC) wastes had the highest concentration. On the other hand, Zarza-Perrunal roasted pyrite ashes (ZP1) presented values similar to those established for unpolluted soils.

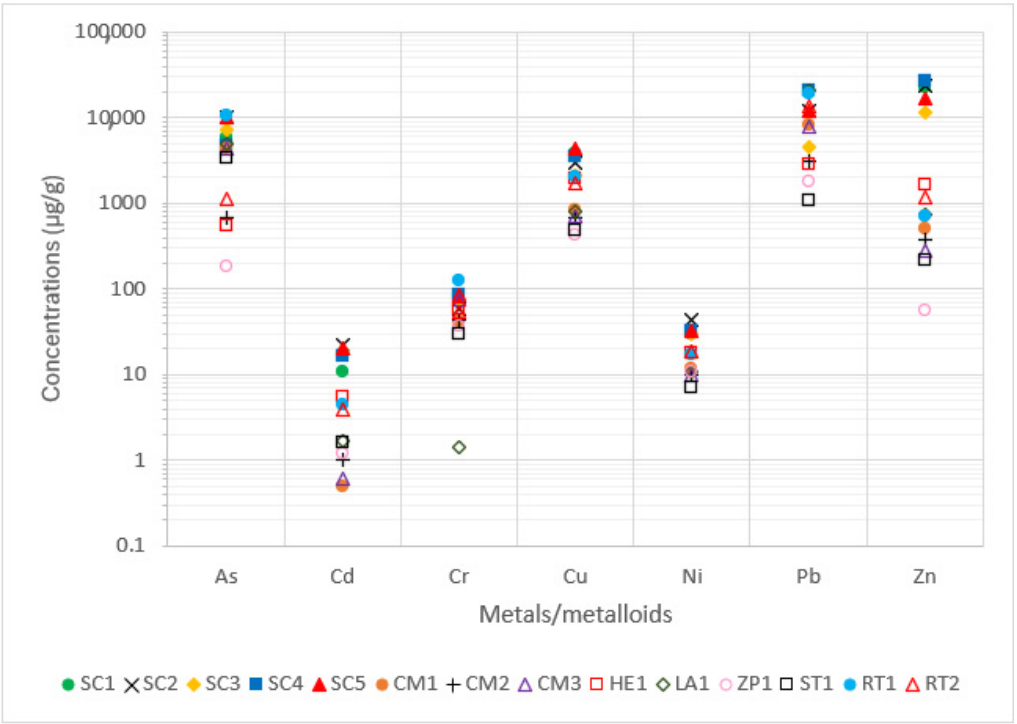

(**a**)

Figure 5. *Cont.*

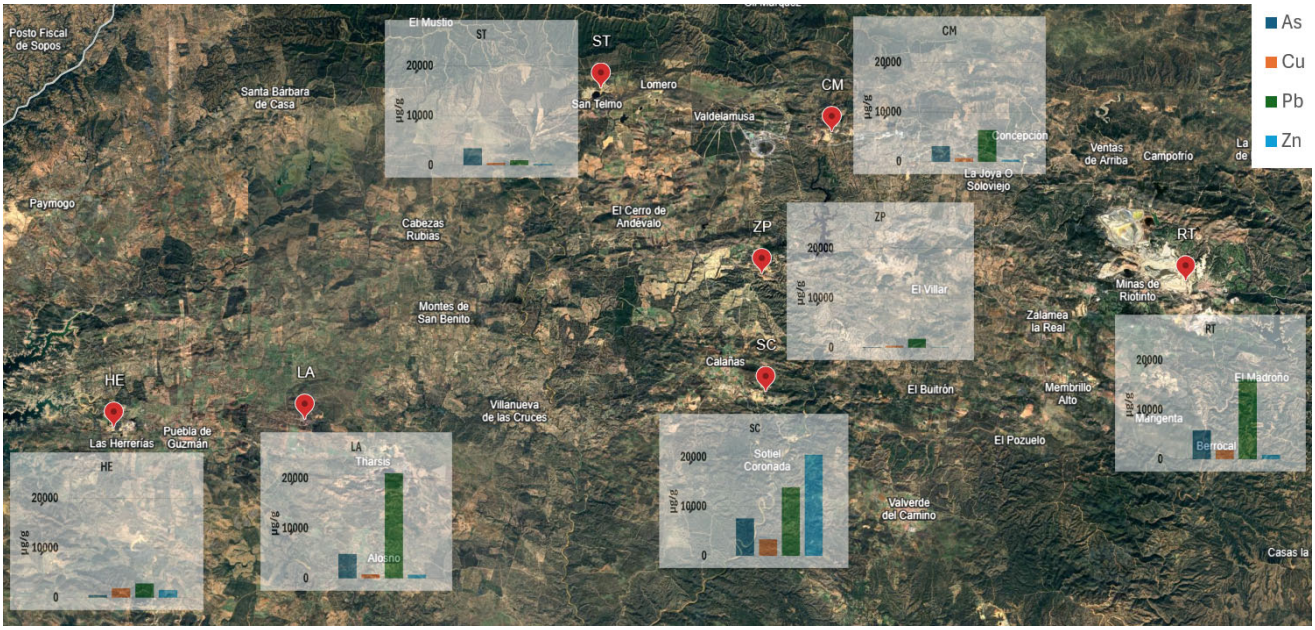

(**b**)

Figure 5. (**a**) Toxic metal/metalloid concentrations (μg/g) in roasted pyrite ash samples. (**b**) Visual map of the average concentrations for As, Cu, Pb, and Zn in the different mines.

For Cd, all wastes had a Cd concentration above the reference 0.12 μg/g [26]. Roasted pyrite ashes from the Cueva de la Mora mine only exceeded them by one order of magnitude, as did Zarza-Perrunal and Lagunazo. The residues from Sotiel Coronada were notable for exceeding them by 2 orders of magnitude. The high toxicity of Cd exposure, such as bone disease and kidney problems, along with the serious danger it poses to the environment and the surroundings, must be emphasized [40]. Finally, Ni and Cr concentrations of the collected samples resembled those expected for a typical soil (37 μg/g and 125 μg/g, respectively [26]), and were even lower in several cases.

As a summary of the previous facts, it is important to point out that these wastes could have a great impact on the environment and require measures for the remediation of these legacy sites to avoid their release into the water systems, as they could reach the human food chain.

3.6. Mineralogy

In order to diagnose the recovery of this waste, it is important to know not only the concentration of major elements but also in which mineralogical form they exist, as future recovery will depend on this fact. The mineralogy of the samples consisted mostly of iron oxides and silica compounds [41]. The mines analyzed by XRD to obtain the mineralogy were those of Sotiel Coronada (SC) and Cueva de la Mora (CM).

Roasted pyrite ash contains an average (see Figure 6) of 64.3% hematite (Fe_2O_3), 9.3% quartz (SiO_2), 5.56% magnetite ($Fe^{2+}Fe^{3+}{}_2O_4$), and 5.43% gypsum ($CaSO^4{\cdot}2H^2O$). The percentage of amorphous phase obtained in the samples was 11.81% on average. There were also other secondary minerals depending on the sample and mining location.

In the wastes from Sotiel Coronada (SC), an amount of around 10% gypsum was observed in all samples. In SC1, SC4, and SC5, a significant amount of magnetite was also detected, between 10% and 20%. For SC2, 7.5% franklinite $(Fe,Mn,Zn)^{2+}(Fe,Mn)^{3+}{}_2O_4$) was also detected. The residues from Cueva de la Mora (CM) had a similar distribution. In CM1, 3.9% kalsilite ($KAlSiO_4$), 0.8% massicot (PbO), and 11% beaverite ($Pb(Fe^{3+}{}_2Zn)(SO_4)_2(OH)_6$) were observed. In CM2, 1.6% zinc sulfide (ZnS) was measured and, in CM3, another 1.6% massicot was detected.

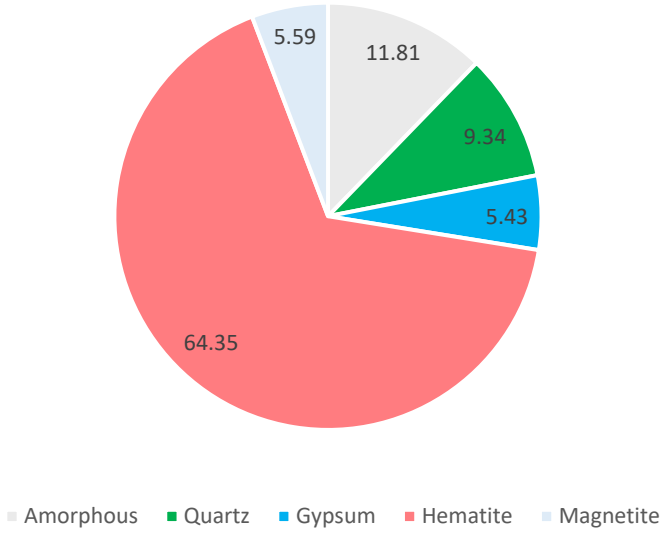

Figure 6. Average mineral concentrations in % of roasted pyrite wastes.

These mineralogical distributions correspond to those previously expected according to the following majority elements obtained: presence of iron oxides such as hematite due to the high Fe (~50%) and O (~30%) content, presence of quartz due to the silicon content (2–8%), presence of minerals with toxic metals/metalloids (Zn and Pb) such as massicot or franklinite, and the existence of gypsum in the Sotiel Coronada residues due to the calcium obtained in some samples (~1.5–2%).

The study of Oliveira's roasted ashes is compatible with our results. They obtained, through XRD, distributions in the range of 73–92% hematite, around 15% magnetite, between 1 and 3% quartz, and, depending on the sample, between 2 and 16% gypsum. It is worth mentioning that the amorphous part was not considered in this study [32].

3.7. Radionuclide Concentrations

For certain applications and environmental impact assessments, it is necessary to analyze the radiological content of the samples. Since mining is considered a NORM activity, the waste generated from roasted pyrite ashes may pose a radiological risk. Therefore, the activity concentrations of natural radionuclides were determined.

Activity concentrations for each waste of the U-series radionuclides are shown in Table 8 including mean values. For the ^{238}U series radionuclides, it can be observed that, for roasted pyrite ashes, all radionuclides had activity concentrations in the same range as expected for soils, i.e., around 30–40 Bqkg^{-1} [23,42]. The only exception was the San Telmo residue (ST1), where the U-series radionuclide concentrations were up to one order of magnitude higher (^{226}Ra = 220 Bqkg^{-1}; ^{238}U = 95 Bqkg^{-1}, and ^{210}Pb = 109 Bqkg^{-1}), indicating that U-series radionuclides were not in secular equilibrium, with these disequilibria being probably due to the previous processes applied on the iron minerals. Considering the obtained standard uncertainties, for most of the samples, there was (or nearly was) secular equilibrium between the long-lived radionuclides of both radioactive series (^{238}U and ^{232}Th). Due to this secular equilibrium in radionuclides, demonstrated through the Sotiel Coronada and Cueva de la Mora mines, not all radionuclides of the radioactive decay series were measured in the following mines in order to speed up the work. In general, the radionuclide concentrations ranged from about 10 Bqkg^{-1} to up to 220 Bqkg^{-1}, with San Telmo being the mine with the highest activity concentrations for U-series.

Table 8. U-series radionuclides activity concentrations for all roasted pyrite ash samples. NM means not measured.

Sample	^{238}U	^{234}Th	^{234}U	^{230}Th	^{226}Ra	^{210}Pb	^{210}Po
SC1	30 ± 3	45 ± 9	31 ± 6	31 ± 3	48 ± 2	45 ± 11	44 ± 3
SC2	34 ± 4	42 ± 9	42 ± 5	77 ± 5	42 ± 2	29 ± 10	1.6 ± 0.6
SC3	26 ± 2	26 ± 7	31 ± 3	36 ± 3	25.0 ± 1.4	8 ± 9	14 ± 3
SC4	26 ± 2	27 ± 8	21 ± 2	43 ± 4	31.1 ± 1.4	22 ± 9	37 ± 4
SC5	41 ± 3	40 ± 7	43 ± 4	53 ± 5	42 ± 2	39 ± 8	30 ± 3
CM1	16 ± 2	11 ± 3	14 ± 2	NM	53 ± 3	36 ± 5	36 ± 1.0
CM2	7 ± 2	10 ± 3	7.6 ± 1.4	NM	14.0 ± 0.8	34 ± 5	38 ± 3
CM3	15 ± 2	12 ± 7	10 ± 2	30 ± 3	34.2 ± 1.4	22 ± 9	25 ± 3
HE1	NM	20 ± 9	NM	NM	15.1 ± 1.4	22 ± 12	NM
LA1	NM	10 ± 3	NM	NM	19.3 ± 1.2	30 ± 4	NM
ZP1	NM	14 ± 3	NM	NM	18.4 ± 1.1	12 ± 4	NM
ST1	NM	95 ± 4	NM	NM	220 ± 8	109 ± 5	NM
RT1	NM	37 ± 4	NM	NM	73 ± 3	40 ± 4	NM
RT2	NM	8 ± 3	NM	NM	36 ± 1.3	19 ± 4	NM
Mean	24.1 ± 0.8	29 ± 3	25 ± 2	45 ± 6	48 ± 2	34 ± 3	19.0 ± 1.1

It should be noted that, in some samples, there are particular cases of disequilibrium between ^{210}Pb and ^{210}Po, and between ^{230}Th and ^{226}Ra (e.g., ST2). This is due to the chemical processes carried out in the mine, which produce the rupture of the secular equilibrium and the enrichment of these two radionuclides. The depletion of ^{210}Pb and ^{210}Po in relation to ^{226}Ra can be justified by considering that their volatility increases with the temperatures of the process, especially above 500 °C, as in the formation of pyrite ashes during the combustion of pyrite [43,44].

Analogously, Table 9 presents the mean activity concentrations of the radionuclides belonging to Th-series and ^{40}K. In the same way as above described, it can be asserted that secular equilibrium was also fulfilled in Th-series. The waste with the highest ^{232}Th-^{228}Ra-^{228}Th activity concentrations was the roasted pyrite ashes from San Telmo, with values between 81 and 94 Bqkg^{-1}. On the other hand, the Zarza Perrunal (ZP) waste had the lowest activity concentrations, very close to the minimum detectable activity, between 2 and 0.56 Bqkg^{-1}. All these values are expected for undisturbed soils, as the Spanish average is 41 Bqkg^{-1} [45].

Table 9. Th-series and ^{40}K radionuclides activity concentrations for all roasted pyrite ash samples. NM means not measured.

Sample	^{232}Th	^{228}Ra	^{228}Th	^{40}K
SC1	82 ± 4	81 ± 3	81.0 ± 2.0	7 ± 6
SC2	68 ± 4	68 ± 3	67.0 ± 1.8	72 ± 9
SC3	64 ± 4	59 ± 3	55.9 ± 1.6	13 ± 2
SC4	55 ± 4	50 ± 3	55.6 ± 1.5	84 ± 8
SC5	50 ± 5	59 ± 3	59.0 ± 1.5	63 ± 7
CM1	NM	8.3 ± 1.2	8.7 ± 0.5	92 ± 6
CM2	NM	2.1 ± 0.8	3.18 ± 0.22	11 ± 3
CM3	7.6 ± 1.4	8.8 ± 1.8	6.3 ± 0.7	61 ± 7
HE1	NM	6.4 ± 0.9	6.4 ± 0.9	32 ± 9
LA1	NM	7.1 ± 1.7	8.3 ± 0.5	67 ± 7
ZP1	NM	2.0 ± 0.9	0.56 ± 0.18	11 ± 4
ST1	NM	81 ± 4	94 ± 4	158 ± 8
RT1	NM	29.9 ± 2.3	27.5 ± 2.0	91 ± 7
RT2	NM	7 ± 3	7.9 ± 0.5	68 ± 6
Mean	54.6 ± 1.2	33.6 ± 1.0	34.1 ± 0.9	59.2 ± 2.1

In the case of ^{40}K, all the activity concentrations obtained were one order of magnitude lower than the Spanish average value, i.e., around 600 Bqkg^{-1} [20]. The highest activity concentration was obtained for ST1 (158 Bqkg^{-1}), while the lowest value was obtained for ZP1 (11 Bqkg^{-1}). ^{235}U was also measured by alpha spectrometry, with activity concentrations averaging 1.5–2.8 Bqkg^{-1}. This is not shown in Figure 4, due to its low relevance. Thus, the roasted pyrite wastes contain activity concentrations of natural radionuclides very similar to those of undisturbed soils.

It is necessary to emphasize the fact that each mine has its own activity concentrations. This can be assumed to be due to the variability of natural terrain (host rocks), and mineralogical processes unique to each mine or storage conditions, if they have suffered from external factors.

3.8. Radon Emanation

Analogously, as previously mentioned, according to European Directive 2013/35/EU, it is necessary to avoid radon gas concentrations above 300 Bqm^{-3} in buildings and structures [4]. If there is a possibility to use these mining wastes as future building materials, the emanation factor and the exhalation rate must be analyzed.

The last radioactive property measured was the Rn emanation factor, through the collection of a composite sample from each mine by mixing the different ashes. The radon accumulation curve is shown in Figure 7. The experimental data can be seen together with the fit. The shaded background corresponds to the measurement errors. The saturation concentration obtained was (29.1 ± 1.3) Bqkg^{-1}. In the same way, the effective time constant obtained was (2.2 ± 0.7)·10^{-5} s^{-1}.

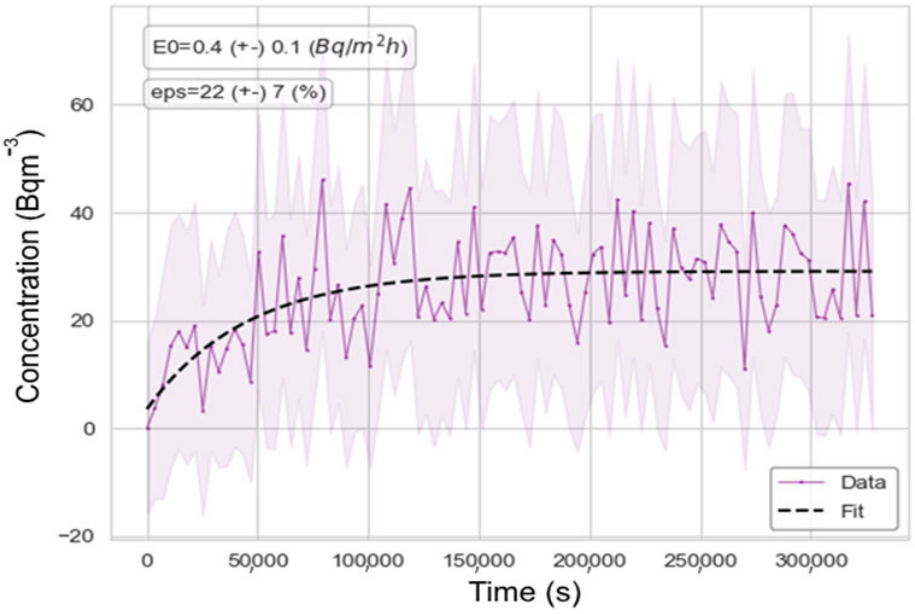

Figure 7. Radon accumulation curve over time, including fit. Pink shadows are error margins of the measurements.

In this way, the emanation factor (ε) and the exhalation rate (E_0) were obtained using Equations (3) and (4). The obtained results were an emanation factor (ε) of (22 ± 7)% and an exhalation rate (E_0) of (0.43 ± 14) Bqm^{-2}h. This emanation factor is within the error range of the emanations obtained by Rogers et al. on different soils (10–30% [46]). According to the classification criteria proposed by Tuccimei on exhalation rates for building materials, this waste belongs to category A (E0 < 0.49 Bqm^{-2}h), thus it would not be a potential source of risk [47].

3.9. Radiological Hazard Indexes

In Table 10, the different radiological hazard indexes are shown for every waste in each mine, including mean values. The calculated indexes were radium equivalent activity (Ra_{eq}), external hazard index (H_{ex}), activity concentration index for gamma radiation emitted by building materials (Ic), and concentration factor for ^{238}U (Fc_{238U}) and ^{232}Th (Fc_{232Th}).

Table 10. Radiological hazard indexes values for Ra_{eq} ($Bqkg^{-1}$), H_{ex}, Ic, Fc_{238U}, and Fc_{232Th}. Mean values included. NM means not measured.

Sample	Ra_{eq}	H_{ex}	Ic	Fc_{238U}	Fc_{232Th}
SC1	161 ± 15	0.44 ± 0.04	0.56 ± 0.02	0.90 ± 0.09	1.94 ± 0.10
SC2	145 ± 14	0.39 ± 0.04	0.50 ± 0.02	1.02 ± 0.12	1.59 ± 0.10
SC3	111 ± 12	0.30 ± 0.03	0.38 ± 0.02	0.77 ± 0.07	1.51 ± 0.08
SC4	106 ± 12	0.29 ± 0.03	0.38 ± 0.02	0.78 ± 0.07	1.29 ± 0.10
SC5	128 ± 11	0.35 ± 0.03	0.46 ± 0.02	1.24 ± 0.10	1.19 ± 0.11
CM1	29 ± 5	0.08 ± 0.01	0.25 ± 0.01	0.50 ± 0.05	NM
CM2	13 ± 4	0.04 ± 0.01	0.06 ± 0.2	0.21 ± 0.05	NM
CM3	29 ± 10	0.08 ± 0.03	0.18 ± 0.02	0.35 ± 0.07	0.18 ± 0.03
HE1	31 ± 11	0.08 ± 0.03	0.09 ± 0.01	0.36 ± 0.06	0.10 ± 0.02
LA1	29 ± 5	0.07 ± 0.02	0.12 ± 0.01	0.56 ± 0.07	0.16 ± 0.03
ZP1	3.8 ± 1.9	0.05 ± 0.01	0.11 ± 0.01	0.26 ± 0.05	0.02 ± 0.05
ST1	128 ± 6	0.60 ± 0.03	1.65 ± 0.07	4.48 ± 0.31	1.30 ± 0.12
RT1	49 ± 4	0.24 ± 0.02	0.58 ± 0.03	1.11 ± 0.12	0.30 ± 0.05
RT2	15 ± 4	0.06 ± 0.02	0.25 ± 0.02	0.59 ± 0.06	0.10 ± 0.02
Mean	70 ± 4	0.22 ± 0.02	0.40 ± 0.02	0.94 ± 0.07	0.81 ± 0.04

The mean Raeq value obtained was 70.0 $Bqkg^{-1}$, which is identical to those that have been previously obtained in soils [48]. The mine with the highest average value was Sotiel Coronada, with 130 $Bqkg^{-1}$, while the mine with the lowest Raeq was Zarza-Perrunal, with 3.8 $Bqkg^{-1}$. All the results in this study were appreciably lower than 370 $Bqkg^{-1}$, which is the world's recommended value as the equivalent to the 1 mSv/y dose rate limit set by the International Commission on Radiation Protection (ICRP) [21]. This result means, as a potential line of valorization, that these wastes can be reused and sold as construction materials.

External hazard index (H_{ex}) values for all samples ranged from 0.04 to 0.60. The highest values were obtained for ST1 waste (0.60), and the lowest values were obtained for CM2 waste (0.04). The mean value obtained was 0.22. All estimated values were lower than the threshold global recommended value (<1). These results imply that the radiation levels measured for these mining wastes do not pose a serious radiological health risk, confirming that exposure to low natural radiation is negligible [21]. A similar analysis was applied for Ic, whose values were in the range between 0.06, for CM2, and 0.58, for RT1 (except for San Telmo waste, ST1). Most wastes had values lower than 1. Thus, as a result, they would comply with Spanish regulations for gamma radiation emitted as construction materials [49]. As a particular case, the Ic obtained for ST1 was 1.65. For this sample, further analysis would not be useful, as it would not comply with the required regulations.

The concentration factors obtained for ^{238}U (Fc_{238U}) were very close to 1 or lower. As previously mentioned, the San Telmo (ST) sample stood out for its high concentration in ^{238}U, thus this factor was 4.48. On the other hand, the Zarza-Perrunal (ZP) sample had a deficit of this radionuclide, with a factor of 0.26. Therefore, it can be ascertained that these wastes have ^{238}U activity concentrations in the range of undisturbed soils. The same justification can be applied to ^{232}Th, as its concentration factors (Fc_{232Th}) ranged from 0.02 for Zarza-Perrunal to 1.50 for Sotiel Coronada (mean value). It can also be stated that the activity concentrations of this radionuclide are typical soil concentrations.

As a summary conclusion, the radiological hazard indexes ratify the results obtained from activity concentration values, affirming that radiological implications of these wastes (direct irradiation) are very low or null. Nevertheless, in waters affected by AMD, high concentrations of both U- and Th-isotopes have been measured, due to the high solubility of these radioelements in the sulfuric acid aqueous medium generated by the AMD processes [50].

3.10. Pollution Indexes

Table 11 shows the different C^i values for the different previously analyzed toxic elements and C_d values for all samples. As, Cu, and Pb contamination factors are notorious for contributing very high levels of pollution in general ($C^i > 6$), exceeding C^i values in some samples by 2 or 3 orders of magnitude for the levels of a typical soil. Exactly the same is true for Zn, except that, in the samples from Cueva de la Mora (CM2 and CM3), the level of contamination was "only" considerable.

Table 11. Contamination factors (C^i) and degrees of contamination (C_d) for the different samples, including means of different wastes. Uncertainties are given as standard deviation of the mean, SD/N1/2, SD—standard deviation of the sampling, N—number of samples.

Sample	C^i (As)	C^i (Cd)	C^i (Cr)	C^i (Cu)	C^i (Ni)	C^i (Pb)	C^i (Zn)	C_d
SC1	1202.1	117.8	0.9	134.6	0.6	1194.1	343.3	2993.4
SC2	2083.3	247.8	0.6	105.0	0.9	700.0	349.3	3486.9
SC3	1514.6	206.7	0.8	75.7	0.6	262.4	173.1	2233.9
SC4	1008.3	185.6	0.9	128.6	0.7	1217.6	404.5	2946.2
SC5	2080.3	231.1	0.9	156.1	0.7	717.6	255.2	3442.0
CM1	910.4	5.6	0.5	30.3	0.3	488.2	7.7	1442.9
CM2	140.2	11.1	0.5	24.3	0.2	182.9	5.7	365.0
CM3	912.5	6.7	0.8	25.4	0.2	458.8	4.2	1408.6
HE1	113	60	0.6	69.3	0.4	168.2	24.2	435
LA1	1022.9	0.4	0.3	167.3	2.3	4375.0	154.2	5722.3
ZP1	37.9	0.3	7.7	89.2	2.3	368.8	11.9	518.0
ST1	708.3	0.3	6.3	100.6	1.5	225.0	45.6	1087.6
RT1	2208.3	0.9	26.7	416.7	3.5	3937.5	144.6	6738.2
RT2	235	0.8	11.5	354.2	4.0	2812.5	247.9	3666.2
Mean	1010 ± 200	80 ± 30	4.2 ± 1.9	130 ± 30	1.3 ± 0.3	1200 ± 400	160 ± 40	2600 ± 500

A similar situation was detected for Ni and Cr. The samples from Sotiel Coronada, Cueva de la Mora, and Herrerías (and Lagunazo in the case of Cr) had a low level of contamination ($C^i < 1$), while, in the rest of the samples, the level was higher (very high for Cr and moderate-considerable for Ni). Cadmium, on the other hand, presented the opposite behavior. The wastes from Lagunazo, Zarza-Perrunal, San Telmo, and Riotinto showed a low level of contamination, and the rest showed a very high level. It is worth mentioning that all samples had a very high contamination degree C_d (>32), specifically 3 orders of magnitude above that of uncontaminated soil. These results illustrate the serious impact of mining waste on the environment, especially for Riotinto-, Lagunazo-, and Sotiel-Coronada-roasted pyrite ash.

Potential ecological risks and ecological risk indexes are shown in Table 12. For arsenic, lead, and copper, as in the previous case, the potential ecological risk of these wastes was extreme ($E^i > 160$). In the same way, Cr and Ni values for Ei in all samples were low ($E^i < 40$), with the exception of the Riotinto wastes, where the risk for Cr was considerable-moderate. In the case of zinc and cadmium, as in the former case, depending on the mine and sample, the risk was one way or another. For zinc, with the exception of Cueva de la Mora and Herrerías, where the risk was low, the rest of the mines had an extreme potential ecological risk for this element. For Cd, the samples from Lagunazo (LA), Zarza-Perrunal (ZP), San

Telmo (ST), and Riotinto (RT) showed a low risk, while, in Sotiel Coronada (SC), Cueva de la Mora (CM), and Herrerías (HE), the risk for this element was extreme. Finally, the ecological risk index was very high for all wastes (RI > 600), specifically several orders of magnitude higher, with RT1 standing out (RI = 67380). Thus, in general, there is an urgent need to consider the serious environmental impact caused by mining waste located in these areas.

Table 12. Potential ecological risk (E^i) and ecological risk index (RI) for the different samples.

Sample	As	Cd	Cr	Cu	Ni	Pb	Zn	Cd
SC1	12,020	3533.3	1.8	673.2	3.2	5970.6	343.3	22,546
SC2	20,833	7433.3	1.3	525.0	4.6	3500.0	349.3	32,646
SC3	15,145	6200.0	1.7	378.6	3.2	1311.8	173.1	23,214
SC4	10,083	5566.7	1.8	642.9	3.4	6088.2	404.5	22,790
SC5	20,830	6933.3	1.8	780.4	3.5	3588.2	255.2	32,392
CM1	9104.2	166.7	0.9	151.4	1.3	2441.2	7.7	11,873
CM2	1402.1	333	0.9	121.6	1.1	914.7	5.7	2779
CM3	9125.0	200	1.7	127.0	1.1	2294.1	4.2	11,753
HE1	1131.3	1800	1.3	346.4	1.9	841.2	24.2	4146
LA1	10,229	3.5	2.9	1672.9	22.9	43,750	1541.7	57,223
ZP1	379.2	2.5	77.1	891.7	22.9	3687.5	118.8	5179
ST1	7083.3	3.3	62.5	1006.3	14.6	2250.0	456.3	10,876
RT1	22,083	9.2	266.7	4166.7	35.4	39,375	1445.8	67,382
RT2	2354.2	8.1	114.6	3541.7	39.6	28,125	2479.2	36,662
Mean	10,100 ± 1900	2300 ± 800	38 ± 20	1000 ± 300	11 ± 4	10,000 ± 4000	540 ± 190	24,000 ± 5000

3.11. Pollutant Mobility

Concentrations of the different anions found in the waters after forced leaching are shown in Table 13. In addition, to make a rigorous comparison, the same process was carried out on a sample of soil from the IPB. The anions that form the generated leachates consist mainly of fluorides (F^-), chlorides (Cl^-), and sulfates (SO_4^{2-}). For fluorides and chlorides, the anion concentrations were in the ranges of 2–37 μg/g and 5–38 μg/g, respectively. These concentrations are far below the limits (500 μg/g fluorides; 25,000 μg/g chlorides) established in R.D. 646/2020 for the acceptance of hazardous waste in landfills [49]. The results are as expected for typical uncontaminated soils. For sulfates, this limit value is at 5.104 μg/g. The wastes from Cueva de la Mora and Sotiel Coronada had sulfate concentrations in the same order of magnitude as this limit, with even sample SC3 exceeding it (6.1.104 μg/g). In roasted pyrite, sulfates are present in the leachates due to the high concentration of S (1–5%) in the ashes [51]. These values, apart from being very close to the limit in several cases, are 2 orders of magnitude higher than those obtained in the soil.

Table 13. Calculated anions concentrations in μg/g for each sample measured by ionic chromatography. NM means not measured.

Sample	Fluoride	Chloride	Sulfate
SC1	2.45	12.09	12,495.59
SC2	7.81	13.18	18,049.06
SC3	36.66	16.45	61,355.42
SC4	8.77	5.70	18,136.36
SC5	8.10	37.87	24,010.59
CM1	2.45	12.09	12,495.59
CM2	5.23	5.00	29,199.09
CM3	3.46	6.06	1567.54
HE1	NM	NM	NM
LA1	5.34	25.72	608.11
ZP1	NM	NM	NM
ST1	NM	NM	NM
RT1	NM	NM	NM
RT2	NM	NM	NM
Mean	8.9 ± 1.2	14.9 ± 1.2	19,800 ± 2000
Soil	3.21	17.22	220.74

The concentrations of the different elements in the leachates of the samples are listed in Figure 8. For uranium and thorium, roasted pyrite ash leachate concentrations did not exceed the International Atomic Energy Agency recommended limits of 3 µg/g. These elements would have low mobility and solubility in this type of waste, obtaining values similar to those found in soils. In the case of Fe, according to the European Union Water Framework Directive (WFD), the limit for Fe in water is 200 µg/g. This value was only exceeded by two samples from Cueva de la Mora, CM1 and CM2, with 346 µg/g and 2281 µg/g, respectively. Moreover, these values were several orders of magnitude higher than the 0.12 µg/g obtained in soil. This may justify the poor roasting process at this mine, due to the existence of soluble secondary minerals such as beaverite ($Pb(Fe^{3+}{}_2Zn)(SO_4)_2(OH)_6$), which is more soluble in acidic conditions, releasing iron into the leachate [52]. The limit according to R.D. 646/2020 for S is 16,600 µg/g, a value only exceeded by SC3.

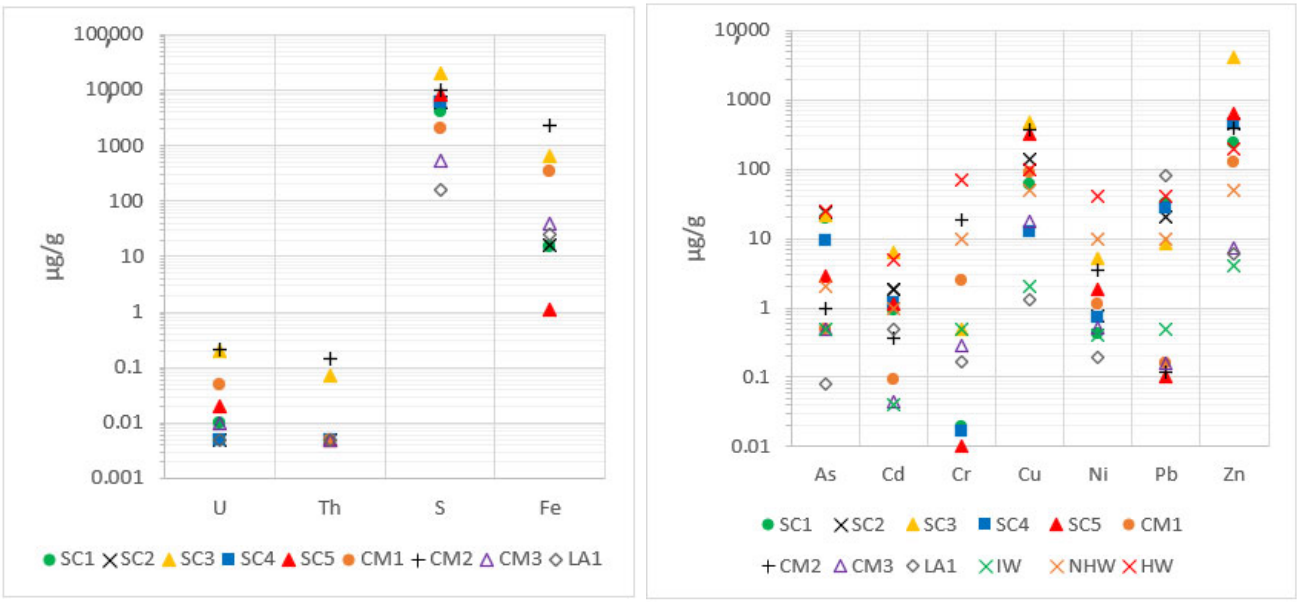

(**a**) (**b**)

Figure 8. (**a**) Elements' leached concentrations for U, Th, Fe, S; (**b**) toxic metals/metalloids' leached concentrations. The classification values according to Decision 2003/33/EC for inert waste (IW), non-hazardous waste (NHW), and hazardous waste (HW) [53] are also included.

Similarly, the seven heavy metals/metalloids with a high toxic component had limits according to Decision 2003/33/EC. These values established by the European Union for classification and admission as hazardous wastes in landfills are as follows: 25 µg/g for As, 5 µg/g for Cd, 70 µg/g for Cr, 100 µg/g for Cu, 40 µg/g for Ni, 50 µg/g for Pb, and 200 µg/g for Zn [53]. For arsenic, chromium, and nickel, no sample exceeded the established limit values. In the case of cadmium and copper, only sample SC3 exceeded the established limits, with concentrations of 6.34 µg/g and 481 µg/g, respectively, indicating a high release of pollutants into the environment by this sample. Similarly, in the case of lead, the values were below the limit, except in LA1, with 79 µg/g. The very high concentration of Pb in this sample affected the release of this element in the same way. Consequently, it is necessary to seek solutions for serious health and environmental problems [54], as soil values for all toxic metals/metalloids were exceeded by several orders of magnitude.

In addition, a previous study by Soriano et al., where a leaching test was performed on roasted pyrite ashes located in Cartagena, provides data of the same order of magnitude for concentrations of toxic metals/metalloids in the leached liquid: 3.8 µg/g for Cd, 1.1 µg/g for Cr, 78 µg/g for Cu, 2.8 µg/g for Ni, 228 µg/g for Pb, and 423 µg/g for Zn. Differences

only exist for lead, where the release in Cartagena waste was one order of magnitude higher [55].

The transfer factors (TF) obtained are shown in Figure 9. The low transfer factors of U (5.1%) and Th (4%) indicate that most of these elements did not pass into the water, remaining in the solid matrix. This limits the potential impact on water, thus reducing the risk of radioactive pollution. As the wastes had a large amount of residual sulfur that had not been burned, due to a not fully efficient roasting process, there would be remains of partially oxidized sulfides, which, under leaching conditions, would oxidize into soluble sulfates. This justifies the large amount of leached S and its high transfer factor (42% on average). The low TF of Fe (0.18%) was due to the presence of insoluble iron oxides such as hematite.

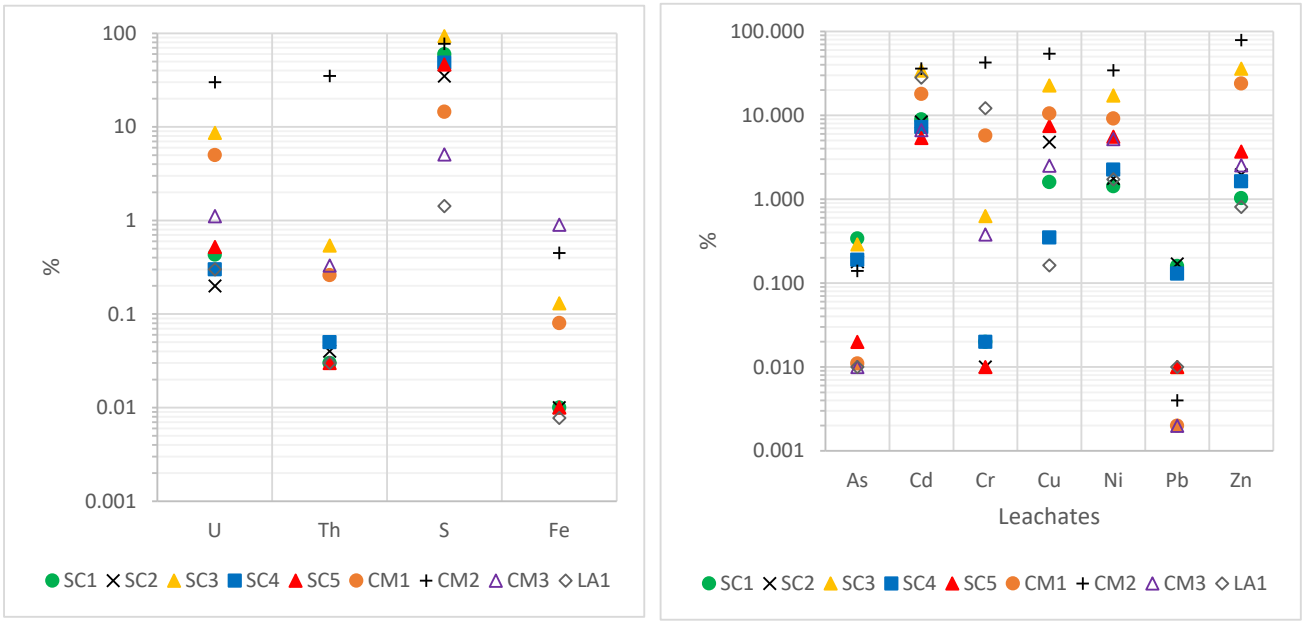

(**a**) (**b**)

Figure 9. (**a**) Transfer factors for U, Th, Fe, S; (**b**) transfer factors for toxic metals/metalloids.

In metals and metalloids, there was a variety of TFs, from 0.06% of Pb to 16.9% of cadmium. Although, for some elements, the fraction of the sample that becomes part of the leachate is small (0.06% for Pb or 0.13% for As), due to the high concentrations, it is necessary to monitor their environmental impact. Concentrations were 2 to 3 orders of magnitude higher than expected for uncontaminated soils, thus, even at low TFs, leachates can cause environmental contamination risks, exceed permitted limits for surface water or groundwater, and affect aquatic organisms.

The mean values of the partition coefficients K_d for each element are provided in Table 14, including ranges and standard deviations. The calculated results for As (405 L/kg), Cr (338 L/kg), Pb (1744 L/kg), and Zn (4.5 L/kg) are similar to K_d obtained in soil sediments established by other studies (140 L/kg, 350 L/kg, 9600 L/kg, and 1.6 L/kg, respectively). These elements have a similar release. However, for U (19.1 L/kg), Th (170.8 L/kg), Fe (724 L/kg), Cd (0.94 L/kg), Cu (11.7 L/kg), and Ni (3.1 L/kg), due to the acidic environment of the waste and leaching, the release and mobility of contaminants was higher, resulting in lower k_d with respect to soils (4000 L/kg, 25,000 L/kg, 25,000 L/kg, 230 L/kg, 780 L/kg, and 980 L/kg, respectively) [56]. According to the mean K_d shown in Table 14, the elements were ordered from highest to lowest mobility:

$$Cd > S > Ni > Zn > Cu > U > Th > Cr > As > Fe > Pb \quad (14)$$

Although the order of mobility of some elements may be characteristic of this waste, comparing the results with those of other studies where the mobility of these pollutants in soils is analyzed, the order is generally similar. In both studies, cadmium is the most mobile element, while arsenic and lead are among the least mobile [57].

Table 14. Partition coefficient K_d obtained in L/kg. Lower and higher values, including mean and standard deviations, are included.

K_d (L/kg)	U	Th	S	Fe	As	Cd	Cr	Cu	Ni	Pb	Zn
Lower Value	0.3	0.2	0.2	11	29.4	0.28	0.23	0.18	0.29	77	0.13
Higher Value	50.0	333.3	7.0	2000	1011	1.50	1007	61.3	6.9	5072	12.3
Mean	19.1	170.8	1.2	724	405	0.94	338	11.7	3.1	1744	4.5
Standard Deviation	5.8	49.4	0.7	234	149	0.19	142	6.9	0.9	665	1.4

4. Valorization Diagnosis

Due to the large quantities of roasted pyrite ashes located in the analyzed mines, along with their implications for the environment and human health, there are many lines of research and development for the valorization of these wastes. The principles of circular economy are implemented by enhancing material flow while considering the potential properties and characteristics of the materials. Some of the methods that have been established over time are shown below.

Considering the presence of hematite in the analyzed pyrite ashes, several studies report that they could be used for the synthesis and production of iron oxide pigments [58,59]. By substituting La^{3+} ion into hematite ($Fe_{2-x}La_xO_3$) from pyrite ashes using a polymeric complex at 1000 °C, it is possible to obtain different shades of colors [60]. Other studies have also used these wastes, with 58% Fe (similar to those used in this study) as a source of secondary raw material in micaceous iron oxide (MIO) pigments. The research developed by Zheng involved processes such as precipitation, leaching, and hydrothermal treatment [61]. The findings indicate that certain physicochemical factors, including NaOH concentrations, total iron content, and reaction temperature, directly influence the morphology and coloration of the pigments produced. Quality tests confirmed that they possessed the essential characteristics required for micaceous iron oxide pigments used in paints (chemical stability, toxicity, durability). The obtained MIO particles were uniform flakes, with 7.0 μm of mean particle size, revealing good crystallization, coinciding with hematite structure [61]. Furthermore, the use of roasted pyrite ashes as pigments has been economically analyzed and shown to be a low-cost process [62].

Moreover, due to the large amount of iron oxides, these wastes have been used as an alternative source of iron in building materials. A study by Alp and co-workers used roasted pyrite ashes with 85% hematite as a source of iron for the production of Portland cement mortars on an industrial scale [63]. Data were collected from all operations for 6 months, analyzing the mineralogical, chemical, and physical properties, such as soundness, fineness, consistency, and lime saturation. Additionally, the mechanical performance for compressive strength of the products obtained from the roasted ashes was also assessed. The results are consistent with those provided by industrial materials with natural iron sources. After a curing period of 28 days, a compressive strength of 43.7 MPa was obtained, which is very similar to the 44 MPa of Fe ore and the 43.0 MPa of CEM I-42.5N. In addition, leaching tests ensured that there was no risk of environmental contamination by release of toxic metals/metalloids. Furthermore, a study by Sola et al. analyzed the use of roasted pyrite ash as a clay substitute in the production of briquettes [64]. Various ash replacement ratios (0–20%) and two sintering temperatures (950 and 1000 °C) were studied by analyzing the bulk densities of the briquettes and the compressive strengths. The results showed that,

when the ratio of pyrite ashes increased in the mixture, there was a regular decrease in bulk density for both sintering temperatures. Compressive strengths of the samples containing pyrite ash mixture were 11.0, 17.5, and 16.5 MPa for ash replacement ratios of 20, 10, and 5%, respectively (for 950 °C), and 21,3, 34.9, and 29.0 MPa, respectively (for 1000 °C). Taking into account that the relevant standard given limits are between 9.8 and 23.54 MPa of the relevant standard, the compressive strength obtained from all samples containing pyrite ash was within these limits [64]. Therefore, there is a real possibility of using these ashes as substitutes in the production of briquettes as building materials at a rate of 10%, based on the compressive strength data. Both studies show economic viability.

In the above cases, iron must be previously extracted and treated in order to be able to carry out these processes. There are several studies and proposals for the recovery of iron from waste or tailings. One applied technique is magnetic separation. By using magnetic separators, which depend on the target mineral to be separated and the composition or the percentage of solid, it is possible to extract minerals such as hematite due to its mild magnetic properties. A study conducted by Sahu in 2022, using a wet high-intensity magnetic separator (WHIMS) and a magnetic field strength of 1.65T, obtained a recovery efficiency of up to 63.4% [65]. Acid leaching has traditionally been regarded as a standard technique for extracting metals from iron tailings. This method is characterized by its streamlined process flow and relatively low initial investment, although it incurs high maintenance expenses. The leaching agents used in this process can be categorized into organic and inorganic acids. Organic acids include citric acid, malic acid, and oxalic acid, while commonly used inorganic acids are sulfuric acid (H_2SO_4), nitric acid (HNO_3), and hydrochloric acid (HCl). Previous work by Wu et al. performed HCl leaching of 6–8% Fe-containing residues. At a pH of 1.5, maintained at 70 °C for 2 h, Fe recovery was 99.3% in the leachates [66]. Finally, another extraction process is flotation. After crushing and grinding to expose the metals, a series of chemical agents, called collectors, are added to help bind the metals to the air bubbles and bring them to the surface [67]. Each method and ore to be extracted requires a very specific collector and extraction conditions. Several studies using different mixing times, collectors, and extraction column roughness have obtained an efficiency of between 50 and 67% for Fe [68,69].

5. Conclusions

This study carried out a radiological, multi-elemental, mineralogical, and contaminant release analysis of roasted pyrite ash wastes from five selected mines located in the Iberian Pyrite Belt. The main conclusions were as follows:

1. The principal mineralogical phases were hematite, magnetite, quartz. and gypsum.
2. The elements present in highest concentrations were Fe (46.4%), Si (5.6%), S (1.2%), and Pb (1.3%), which were, in general, several orders of magnitude higher than those found in uncontaminated soils. This fact results in extreme potential ecological risk factors in many samples, which can generate high risks in several work and public activities developed in the surroundings of these areas.
3. The natural radionuclide concentrations of both ^{238}U and ^{232}Th decay series were similar to typical undisturbed soils, with averages around 24 $Bqkg^{-1}$ for ^{238}U, and 55 $Bqkg^{-1}$ for ^{232}Th. Nevertheless, ^{40}K levels were one order of magnitude lower than those of unperturbed soils (around 60 $Bqkg^{-1}$).
4. No secular equilibrium between ^{210}Pb and ^{226}Ra was found, justified by the very high volatility of Pb under the high temperatures that are reached in pyrite roasting.
5. The radiological hazard indexes were one order of magnitude lower than the threshold recommended by international institutions; therefore, the use of these wastes in valorization processes does not have radiological implications.

6. The radon emanation factor of the waste was also measured, being comparable to that of unperturbed soils, presenting an emanation factor of 22 ± 7%.
7. Different valorization options were analyzed for this mining waste, and the following options were proposed: (1) source of iron in cement production or for pigment additives; (2) source of Fe for producing $FeCl_3$ and $FeSO_4$; and (3) substitute for clays in the production of briquettes or bricks.

Author Contributions: Conceptualization, J.P.B.; methodology, J.A.R.-P., M.J.G.-G. and J.P.B.; software, J.A.R.-P.; validation, M.J.G.-G. and J.P.B.; formal analysis, J.P.B.; investigation, J.A.R.-P., M.J.G.-G. and J.P.B.; resources, J.P.B.; data curation, J.A.R.-P.; writing—original draft preparation, J.A.R.-P.; writing—review and editing, J.A.R.-P.; visualization, M.J.G.-G. and J.P.B.; supervision, M.J.G.-G. and J.P.B.; project administration, J.P.B.; funding acquisition, J.P.B. All authors have read and agreed to the published version of the manuscript.

Funding: This research was funded by the Spanish State Agency whose name is "Diagnosis and proposals for the environmental recovery of areas affected by industrial and mining activities; Implications for the Huelva estuary (RESTOREHU), Ref.: TED2021-130361B-I00)", grants PID2020-116461RB-C21 and 116461RA-C22) funded by MICIU/AEI/10.13039/501100011033.

Data Availability Statement: The original contributions presented in this study are included in the article. Further inquiries can be directed to the corresponding author.

Conflicts of Interest: The authors declare no conflict of interest.

References

1. Inverno, C.; Díez-Montes, A.; Rosa, C.; García-Crespo, J.; Matos, J.; García-Lobón, J.L.; Carvalho, J.; Bellido, F.; Castello-Branco, J.M.; Ayala, C.; et al. Introduction and geological setting of the Iberian Pyrite Belt. In *3D, 4D and Predictive Modelling of Major Mineral Belts in Europe*; Springer: Berlin/Heidelberg, Germany, 2015; pp. 191–208.
2. Yesares, L.; González-Jiménez, J.M.; Jiménez-Cantizano, F.A.; González-Pérez, I.; Caro-Moreno, D.; Sánchez, I.M. Unveiling High-Tech Metals in Roasted Pyrite Wastes from the Iberian Pyrite Belt, SW Spain. *Sustainability* **2023**, *15*, 12081. [CrossRef]
3. Grande, J.A.; De la Torre, M.L.; Cerón, J.C.; Beltrán, R.; Gómez, T. Overall hydrochemical characterization of the Iberian Pyrite Belt. Main acid mine drainage-generating sources (Huelva, SW Spain). *J. Hydrol.* **2010**, *390*, 123–130. [CrossRef]
4. Valente, T.; Grande, J.A.; De La Torre, M.L.; Santisteban, M.; Cerón, J.C. Mineralogy and environmental relevance of AMD-precipitates from the Tharsis mines, Iberian Pyrite Belt (SW, Spain). *Appl. Geochem.* **2013**, *39*, 11–25. [CrossRef]
5. European Commission. Directorate-General Environment: Practical Use of the Concepts of Clearance and Exemption—Part II: Application of the Concepts of Exemption and Clearance to Natural Radiation Sources. In *Radiation Protection 122*; European Commission: Luxembourg, 2002.
6. Lee, J.; Kim, Y.-J.; Chae, J.-S.; Oh, J.S.; Kwon, E.; Lim, J.-M.; Lee, H.; Han, J.H.; Pham, M.K.; Nour, S.; et al. Preparation and evaluation of new reference materials for naturally occurring radioactive materials (NORM): Zirconium silicate, bauxite, and phosphogypsum. *Appl. Radiat. Isot.* **2021**, *168*, 109525. [CrossRef]
7. Álvarez-Valero, A.M.; Sáez, R.; Pérez-López, R.; Delgado, J.; Nieto, J.M. Evaluation of heavy metal bio-availability from Almagrera pyrite-rich tailings dam (Iberian Pyrite Belt, SW Spain) based on a sequential extraction procedure. *J. Geochem. Explor.* **2009**, *102*, 87–94. [CrossRef]
8. Karachaliou, T.; Protonotarios, V.; Kaliampakos, D.; Menegaki, M. Using risk assessment and management approaches to develop cost-effective and sustainable mine waste management strategies. *Recycling* **2016**, *1*, 328–342. [CrossRef]
9. Figueredo, J.L.; Guillén, J.; Salas, A.; Tejado, J.J.; Muñoz-Muñoz, J.G.; Caballero, J.M. Assessment of environmental radiological impact in former metallic mines in Extremadura (Spain): A case study. *J. Environ. Radioact.* **2024**, *275*, 107412. [CrossRef]
10. Hierro, A.; Bolivar, J.P.; Vaca, F.; Borrego, J. Behavior of natural radionuclides in surficial sediments from an estuary impacted by acid mine discharge and industrial effluents in Southwest Spain. *J. Environ. Radioact.* **2012**, *110*, 13–23. [CrossRef]
11. Runkel, M.; Sturm, P. Pyrite roasting, an alternative to sulphur burning. *J. South. Afr. Inst. Min. Metall.* **2009**, *109*, 491–496.
12. Le Saoût, G.; Kocaba, V.; Scrivener, K. Application of the Rietveld method to the analysis of anhydrous cement. *Cem. Concr. Res.* **2011**, *41*, 133–148. [CrossRef]
13. Pérez-Moreno, S.M.; Gázquez, M.J.; Pérez-López, R.; Bolivar, J.P. Validation of the BCR sequential extraction procedure for natural radionuclides. *Chemosphere* **2018**, *198*, 397–408. [CrossRef] [PubMed]
14. Barba-Lobo, A.; Mosqueda, F.; Bolívar, J.P. An upgraded lab-based method to determine natural γ-ray emitters in NORM samples by using Ge detectors. *Measurement* **2021**, *186*, 110153. [CrossRef]

15. Barba-Lobo, A.; Gutiérrez-Álvarez, I.; San Miguel, E.G.; Bolívar, J.P. A methodology to determine 212Pb, 212Bi, 214Pb and 214Bi in atmospheric aerosols; Application to precisely obtain aerosol residence times and Rn-daughters' equilibrium factors. *J. Hazard. Mater.* **2023**, *445*, 130521. [CrossRef]
16. Castaño-Casco, E.; Caño, A.; Suárez-Navarro, J.A.; Gutiérrez-Álvarez, I.; Barba-Lobo, A.; Bolívar, J.P.; Alonso, M.D.M. Radon diffusion coefficient of cement pastes made with recycled thermal carbon fly ashes. *Constr. Build. Mater.* **2025**, *458*, 139556. [CrossRef]
17. Gutiérrez-Álvarez, I.; Martín, J.E.; Adame, J.A.; Grossi, C.; Vargas, A.; Bolívar, J.P. Applicability of the closed-circuit accumulation chamber technique to measure radon surface exhalation rate under laboratory conditions. *Radiat. Meas.* **2020**, *133*, 106284. [CrossRef]
18. Ahmed, R.S.; Mohammed, R.S.; Abdaljalil, R.O. The activity concentrations and radium equivalent activity in soil samples collected from the eastern part of Basrah Governorate in Southern Iraq. *Int. J. Anal. Chem.* **2018**, *1*, 2541020. [CrossRef]
19. da Silva, L.B.; da Silva, L.F.; Orejuela, C.O.P.; Junior, V.B.; da Silva, A.X. Assessment and estimation of the effective dose due to external exposure from natural radioactivity of sands used in civil construction in the state of Rio de Janeiro, Brazil. *Appl. Radiat. Isot.* **2024**, *205*, 111157. [CrossRef]
20. Charles, M. UNSCEAR Report 2000: Sources and effects of ionizing radiation. *J. Radiol. Prot.* **2001**, *21*, 83–85. [CrossRef]
21. Eke, B.C.; Akomolafe, I.R.; Ukewuihe, U.M.; Onyenegecha, C.P. Assessment of radiation hazard indices due to natural radionuclides in soil samples from Imo State University, Owerri, Nigeria. *Environ. Health Insights* **2024**, *18*, 11786302231224581. [CrossRef]
22. Oluyide, S.O.; Tchokossa, P.; Orosun, M.M.; Akinyose, F.C.; Louis, H.; Ige, S.O. Natural radioactivity and radiological impact assessment of soil, food and water around iron and steel smelting area in Fashina Village, Ile-Ife, Osun State, Nigeria. *J. Appl. Sci. Environ. Manag.* **2019**, *23*, 135–143. [CrossRef]
23. Rudnick, R.L.; Gao, S. *Readings from the Treatise on Geochemistry*; Elsevier: Amsterdam, The Netherlands, 2010; Volume 131.
24. Vineethkumar, V.; Sayooj, V.V.; Shimod, K.P.; Prakash, V. Estimation of pollution indices and hazard evaluation from trace elements concentration in coastal sediments of Kerala, Southwest Coast of India. *Bull. Natl. Res. Cent.* **2020**, *44*, 198. [CrossRef]
25. Hakanson, L. An ecological risk index for aquatic pollution control. A sedimentological approach. *Water Res.* **1980**, *14*, 975–1001. [CrossRef]
26. Gao, S.; Rudnick, R.L.; Yuan, H.-L.; Liu, X.-M.; Liu, Y.-S.; Xu, W.-L.; Ling, W.-L.; Ayers, J.; Wang, X.-C.; Wang, Q.-H. Recycling lower continental crust in the North China craton. *Nature* **2004**, *432*, 892–897. [CrossRef]
27. Zandi, M.; Russell, N.V.; Edyvean, R.G.; Hand, R.J.; Ward, P. Interpretation of standard leaching test BS EN 12457-2: Is your sample hazardous or inert? *J. Environ. Monit.* **2007**, *9*, 1426–1429. [CrossRef]
28. Boithias, L.; Sauvage, S.; Merlina, G.; Jean, S.; Probst, J.L.; Pérez, J.M.S. New insight into pesticide partition coefficient Kd for modelling pesticide fluvial transport: Application to an agricultural catchment in south-western France. *Chemosphere* **2014**, *99*, 134–142. [CrossRef]
29. Martín-Méndez, I.; Llamas Borrajo, J.; Bel-lan, A.; Locutura, J. Geochemical distribution in residual soils of Iberian Pyrite Belt (Spain). *J. Iber. Geol.* **2023**, *49*, 97–114. [CrossRef]
30. López, M.; González, I.; Romero, A. Trace elements contamination of agricultural soils affected by sulphide exploitation (Iberian Pyrite Belt, SW Spain). *Environ. Geol.* **2008**, *54*, 805–818. [CrossRef]
31. Pandit, P.; Mangala, P.; Saini, A.; Bangotra, P.; Kumar, V.; Mehra, R.; Ghosh, D. Radiological and pollution risk assessments of terrestrial radionuclides and heavy metals in a mineralized zone of the siwalik region (India). *Chemosphere* **2020**, *254*, 126857. [CrossRef]
32. Oliveira, M.L.; Ward, C.R.; Izquierdo, M.; Sampaio, C.H.; de Brum, I.A.; Kautzmann, R.M.; Sabedot, S.; Querol, X.; Silva, L.F. Chemical composition and minerals in pyrite ash of an abandoned sulphuric acid production plant. *Sci. Total Environ.* **2012**, *430*, 34–47. [CrossRef]
33. Guney, M.; Karatas, T.; Ozkul, C.; Akyol, N.H.; Acar, R.U. Contamination by As, Hg, and Sb in a region with geogenic As anomaly and subsequent human health risk characterization. *Environ. Monit. Assess.* **2020**, *192*, 50. [CrossRef]
34. Zhao, F.; Gu, S.; Li, Q.; Guo, Z.; Zhang, X.; You, G.; Deng, G.; Zhang, T. Persistent thallium enrichment and its high ecological risks developed from historical carbonaceous Hg-Tl mining waste. *Sci. Total Environ.* **2023**, *902*, 166068. [CrossRef] [PubMed]
35. Rosario-Beltré, A.J.; Sánchez-España, J.; Rodríguez-Gómez, V.; Fernández-Naranjo, F.J.; Bellido-Martín, E.; Adánez-Sanjuán, P.; Arranz-González, J.C. Critical Raw Materials recovery potential from Spanish mine wastes: A national-scale preliminary assessment. *J. Clean. Prod.* **2023**, *407*, 137163. [CrossRef]
36. O'Neill, H.S.C. The smoothness and shapes of chondrite-normalized rare earth element patterns in basalts. *J. Petrol.* **2016**, *57*, 1463–1508. [CrossRef]
37. Gao, S.; Luo, T.C.; Zhang, B.R.; Zhang, H.F.; Han, Y.W.; Zhao, Z.D.; Hu, Y.K. Chemical composition of the continental crust as revealed by studies in East China. *Geochim. Cosmochim. Acta* **1988**, *62*, 1959–1975. [CrossRef]

38. Pyrgaki, K.; Gemeni, V.; Karkalis, C.; Koukouzas, N.; Koutsovitis, P.; Petrounias, P. Geochemical occurrence of rare earth elements in mining waste and mine water: A review. *Minerals* **2021**, *11*, 860. [CrossRef]
39. Fávaro, D.I.T. Distribution of U and Th decay series and rare earth elements in sediments of Santos Basin: Correlation with industrial activities. *J. Radioanal. Nucl. Chem.* **2005**, *264*, 449–455. [CrossRef]
40. Järup, L.; Åkesson, A. Current status of cadmium as an environmental health problem. *Toxicol. Appl. Pharmacol.* **2009**, *238*, 201–208. [CrossRef]
41. Raasch, D. Magneto-optic Recording Materials: Chemical Stability and Life Time. In *Encyclopedia of Materials: Science and Technology*; Elsevier: Amsterdam, The Netherlands, 2001; pp. 5061–5063. Available online: https://ui.adsabs.harvard.edu/link_gateway/2001emst.book.5061R/doi:10.1016/B0-08-043152-6/00877-9 (accessed on 17 October 2024).
42. Guerrero, J.L.; Barba-Lobo, A.; Romero-Forte, C.; Bolívar, J.P. Assessment of metal(loid) and natural radionuclide pollution in surface sediments of an estuary affected by mining and phosphogypsum releases. *Environ. Sci. Pollut. Res.* **2024**, *31*, 51489–51503. [CrossRef]
43. Długosz-Lisiecka, M.; Perka, D. Modeling of 210 Pb and 210 Po radionuclide emissions from local power plants in central Poland. *Environ. Sci. Process. Impacts* **2020**, *22*, 2291–2297. [CrossRef]
44. Mora, J.C.; Robles, B.; Corbacho, J.A.; Gascó, C.; Gázquez, M.J. Modelling the behaviour of 210Po in high temperature processes. *J. Environ. Radioact.* **2011**, *102*, 520–526. [CrossRef]
45. Quindos, L.S.; Fernandez, P.L.; Soto, J.; Rodenas, C.; Gomez, J. Natural radioactivity in Spanish soils. *Health Phys.* **1994**, *66*, 194–200. [CrossRef] [PubMed]
46. Rogers, V.C.; Nielson, K.K.; Kalkwarf, D.R. *Radon Attenuation Handbook for Uranium Mill Tailings Cover Design*; NUREG/CR-3533; PNL-4878; RAE-18-5; ON: DE84011549; Rogers and Associates Engineering Corporation: Salt Lake City, UT, USA, 1984. [CrossRef]
47. Tuccimei, P.; Castelluccio, M.; Soligo, M.; Moroni, M. Radon exhalation rates of building materials: Experimental, analytical protocol and classification criteria. In *Building Materials: Properties, Performance and Applications*; Nova Science Publishers, Inc.: Hauppauge, NY, USA, 2009; pp. 259–274.
48. dos Santos Júnior, J.A.; de Araújo, E.E.N.; Fernández, Z.H.; dos Santos Amaral, R.; do Nascimento Santos, J.M.; Milán, M.O. Measurement of natural radioactivity and radium equivalent activity for pottery making clay samples in Paraíba and Rio Grande do Norte–Brazil. *Environ. Adv.* **2021**, *6*, 100121. [CrossRef]
49. Santos, Á.M.; Teresa, L.C.A.; Llácer, J.M.M.; Romero, M.I.; Manjón, M.D.M.P.P.; del Llano, S.L.L. *Real Decreto 1029/2022, de 20 de Diciembre, por el que se Aprueba el Reglamento Sobre Protección de la Salud Contra los Riesgos Derivados de la Exposición a las Radiaciones Ionizantes: ¿Preguntas y Respuestas?* Agencia Estatal Boletín Oficial del Estado: Madrid, Spain, 2022.
50. Manjón, G.; Mantero, J.; Vioque, I.; Galván, J.; Díaz-Francés, I.; García-Tenorio, R. Some naturally occurring radionuclides (NORM) in a river affected by acid mining drainages. *Actual. Jurídica Ambient.* **2021**, *108*, 52–64. [CrossRef]
51. Chandra, A.P.; Gerson, A.R. The mechanisms of pyrite oxidation and leaching: A fundamental perspective. *Surf. Sci. Rep.* **2010**, *65*, 293–315. [CrossRef]
52. Jambor, J.L.; Dutrizac, J.E. The synthesis of beaverite. *Can. Mineral.* **1985**, *23*, 47–51.
53. *Decisión 2003/33/CE*; Official Journal of the European Communities. European Union: Brussels, Belgium, 2003.
54. Demır, G.; Çoruh, S.; Ergun, O.N. Leaching behavior and immobilization of heavy metals in zinc leach residue before and after thermal treatment. *Environ. Prog.* **2008**, *27*, 479–486. [CrossRef]
55. Soriano-Disla, J.M.; Spille, U.; Gabarrón, M.; Faz, Á.; Acosta, J.A. Evaluation of strategies for mitigating risks associated with metals in pyrite ash. *Environ. Manag.* **2018**, *2017*, 403–410. [CrossRef]
56. Sheppard, S.; Long, J.; Sanipelli, B.; Sohlenius, G. *Solid/liquid Partition Coefficients (Kd) for Selected Soils and Sediments at Forsmark and Laxemar-Simpevarp*; Swedish Nuclear Fuel and Waste Management Co.: Stockholm, Sweden, 2009; No. SKB-R--09-27.
57. Clemente, R.; Dickinson, N.M.; Lepp, N.W. Mobility of metals and metalloids in a multi-element contaminated soil 20 years after cessation of the pollution source activity. *Environ. Pollut.* **2008**, *155*, 254–261. [CrossRef]
58. Liu, Z.; Zheng, Y. Effect of Fe (II) on the formation of iron oxide synthesized from pyrite cinders by hydrothermal process. *Powder Technol.* **2011**, *209*, 119–123. [CrossRef]
59. Nicoleta Codreanu, A.M.; Constantin, A.; Kim, L.; Gasnac, G.G. An overview of the most actual methods of pyrite ash valorization. *Rom. J. Ecol. Environ. Chem.* **2022**, *4*, 97–103. [CrossRef]
60. Bhuiyan, T.I.; Nakanishi, M.; Kusano, Y.; Fujii, T.; Takada, J.; Ikeda, Y. Synthesis, morphology and color tone properties of the lanthanum substituted hematite. *Mater. Lett.* **2007**, *61*, 3774–3777. [CrossRef]
61. Zheng, Y.; Liu, Z. Preparation of monodispersed micaceous iron oxide pigment from pyrite cinders. *Powder Technol.* **2007**, *207*, 335–342. [CrossRef]
62. Allen, R.L. *Colour Chemistry*; Springer Science & Business Media: Berlin, Germany, 2013.
63. Alp, I.; Deveci, H.; Yazıcı, E.; Türk, T.; Süngün, Y. Potential use of pyrite cinders as raw material in cement production: Results of industrial scale trial operations. *J. Hazard. Mater.* **2009**, *166*, 144–149. [CrossRef]

64. Sola, O.C.; Atis, C.D. The effects of pyrite ash on the compressive strength properties of briquettes. *KSCE J. Civ. Eng.* **2012**, *16*, 1225–1229. [CrossRef]
65. Sahu, S.N.; Meikap, B.C.; Biswal, S.K. Magnetization roasting of waste iron ore beneficiation plant tailings using sawdust biomass; A novel approach to produce metallurgical grade pellets. *J. Clean. Prod.* **2022**, *343*, 130894. [CrossRef]
66. Wu, Z.; Deng, J.; Zhao, T.; Zhou, Y.; Kang, Y.; Bai, X.; Hong, F.; Fu, L.; Li, G.; Zhang, Z.; et al. Transforming Mining Waste to Wealth: A Novel Process for the Sustainable Recovery and Utilization of Iron Tailings through HCl Leaching and MOFs Absorption. *Sustainability* **2024**, *16*, 1945. [CrossRef]
67. Mu, Y.; Peng, Y.; Lauten, R.A. The depression of pyrite in selective flotation by different reagent systems–A Literature review. *Miner. Eng.* **2016**, *96*, 143–156. [CrossRef]
68. Rocha, L.; Cançado, R.Z.L.; Peres, A.E.C. Iron ore slimes flotation. *Miner. Eng.* **2010**, *23*, 842–845. [CrossRef]
69. Pereira, A.R.M.; Hacha, R.R.; Torem, M.L.; Merma, A.G.; Silvas, F.P. Direct hematite flotation from an iron ore tailing using an innovative biosurfactant. *Sep. Sci. Technol.* **2021**, *56*, 2978–2988. [CrossRef]